Understanding the Middle Miocene Climatic Optimum: Evaluation of Deuterium Values (δD) Related to Precipitation and Temperature

The Honors Program

Senior Capstone Project

Student's Name: Colin Gannon

Faculty Sponsor: Hong Yang

April, 2013

Table of Contents

Understanding the Middle Miocene Climatic Optimum: Evaluation of Deuterium Values (δD) Related to Temperature and Precipitation

Colin Gannon[1], Brian Blais[1,2], Qin Leng[1], Robert Patalano[1], Hong Yang[1]

[1]Laboratory for Terrestrial Environments, Department of Science and Technology, College of Arts and Science, Bryant University, Smithfield, RI, USA; [2]Institute for Brain and Neural Systems, Brown University, Providence, RI, USA

FOREWORD

Reading this Capstone

This capstone is organized in the form of a scientific journal article and has been written with intent to submit as a publication. The Abstract, Introduction, Methods, Data Analysis, Discussion, and Conclusion sections thoroughly outline the process of preparing samples for evaluation, and subsequent interpretations of the relationship between the data and the Middle Miocene Climatic Optimum.

This Foreword, along with the Afterword and Appendices following the manuscript, have all been included for the benefit of this Honors Capstone to provide a background of the overall concepts of this research. For any unfamiliar vocabulary, please refer to Appendix A, which contains a full glossary of the technical terms used throughout this manuscript.

Background

Understanding and forecasting climate, even with modern day technology and supercomputers, is a dauntingly complex task. The climate of any given location is inextricably connected to myriad factors, susceptible to change with any fluctuation in a multitude of variables. To illustrate climate dynamics, it is best to begin by breaking down the Earth into "spheres." These include the atmosphere, biosphere, hydrosphere, and geosphere, each having many sub-divisions themselves. These spheres have been evaluated by the scientific community thoroughly, their physical features identified, helping us to understand the dynamics of each. These spheres are deeply interconnected, and it is when these linkages are studied that we can begin to elucidate climate on a larger scale.

In recent years, climate change and global warming have been under scrutiny from main stream media, politicians, the general public, and the scientific community alike. Incidentally, much of the attention is in the form of confusion and debate over the drivers of the change, and the extent of its consequences. It is not surprising that there is a high degree of ambiguity, as understanding global climate at the macro-level involves interpreting millions of data points from all across the world, and accurately assigning mathematical approximations to represent physical processes in the atmosphere. Global circulation models (GCMs) attempt to take massive data fields and interpret them by inputting them into hundreds of formulas to predict the magnitude to which a variation in one variable will affect climate. This extremely sophisticated method is not only very expensive to execute, but is often riddled with holes and flaws. Regardless, this is the best method to date for simulating modern climate and forecasting future fluctuations.

Another issue with understanding present and future climates is the lack of understanding that specific variables have on influencing climate on a large scale. As outlined earlier, there are four major spheres of the Earth, each having a substantial impact on climate. Each sphere is comprised of many dynamics and factors, each of varying weight in changing precipitation and temperature at a given location and time. An example of this, which has received a great deal of media attention lately, is the atmospheric carbon dioxide (CO_2) concentration. In the context of climate change, carbon dioxide is a "greenhouse gas" in the atmosphere which prevents heat from escaping the Earth, causing surface temperatures to rise. It is a natural product of organism respiration, wildfire burning, and emission from deep Earth through volcanoes, hot springs, and geysers. But after the human industrial revolution, it has been released at a faster rate from human activities such as combustion of fossil fuels. The levels of greenhouse gases in the atmosphere have fluctuated drastically over time, increasing dramatically in the last century or so, and it has been demonstrated that there is a correlation between the amount of greenhouse gases in the atmosphere and temperature (Solomon, 2007). However, despite a great deal of research and discussion, the exact degree to which CO_2 levels influence temperature is not perfectly understood. Although there are almost certainly some correlations, it is by no means a directly proportional relationship, as countless other factors must be considered.

The objective of modern climate research is to evaluate specific variables, such as CO_2, and identify the significance it has in influencing global climate. While it is relatively plausible to construct the present day climate through data collection and then model simulation, it is more difficult to delineate the extent to which any one piece of data relates to other environmental and climatic variables. To truly gain insight into these correlations, we must look back to past climates and attempt to reconstruct the interconnections. This is done through the evaluation of direct evidence and/or indirect proxy data. As far as atmospheric CO_2 concentration is concerned, its direct evidence can be obtained from air bubbles trapped in ice cores to directly trace carbon dioxide levels in the ancient atmosphere from up to nearly one million years ago (White, 2004). However, for climate into geological times, proxies are needed. A proxy is anything that remains from a past climate that can be used as evidence to indirectly reconstruct the conditions during the time (Moberg et al., 2005).

Analyzing proxy data for paleoclimates, or ancient climates, is crucial to forecasting how the modern day climate will shift as certain variables fluctuate. As data accumulates from all of the Earth's past climates (extending back millions of years), there is more accuracy in predicting how the Earth will respond to changes brought upon it. Although the process is complex, it must be broken down into small pieces from which we can raise our level of precision. The world today is faced with a rapidly changing global climate; knowing the significance of fluctuations of all variables is crucial to modeling the change and inferring its consequences. With a more accurate model, we will be better prepared to mitigate and adapt to the changing climate.

About Our Research

Considering the above discussion, this Honors Capstone sets out to analyze an ancient climate and model on how a unique atmospheric dynamic influenced a particular aspect of the climate. Specifically, we look at how a reduced latitudinal temperature gradient impacted evaporation and precipitation. That is, in a climate with a small temperature difference between the Equator and the poles (relative to modern day), how was the relationship between evaporation and precipitation influenced? It has been established by the scientific community that there was a reduced temperature gradient during middle Miocene time (about 15 -17 million years ago, a time known as the Middle Miocene Climate Optimum (MMCO) (Böhme, 2003); however, little

is known about the impact this climate event had on evaporation and precipitation. Our research aims to provide insight towards these relationships. With a better understanding of how temperature impacts evaporation and precipitation at any given location during this period, we not only help to reconstruct ancient climate, but also predict how a future climate with similar conditions might behave.

As this is a paleoclimatic study, we were dependent upon proxy data to create our model. Our proxy was deuterium and hydrogen ratio (δD) on plant lipids from well-preserved fossils and sediments. Deuterium is an isotope of hydrogen and is present, albeit in low abundance, in nature (water, biomolecules, etc). In a given precipitation sample, the amount of deuterium is dependent upon a few factors, most importantly latitude, precipitation, and atmospheric temperature (Dansgaard, 1964; Gat, 1996; Jouzel, 1997). Therefore, by evaluating the ratio at a given location, it is possible to reconstruct several atmospheric characteristics. The exact methods by which this is executed are explained within the scope of this Capstone.

The paleoclimate condition which we chose to evaluate occurred during a geologic time period known as the "Miocene" epoch, which spanned from approximately 23 to 5.33 million years ago (Ma) (Geologic Time Scale Foundation, 2012). A unique geologic time period referred to as the "Middle Miocene Climatic Optimum (“MMCO”) occurred about 15-17 Ma (Böhme, 2003). During this time the Earth warmed rapidly, with similarities to the way the modern climate's temperature is changing. This research evaluates hydrogen isotope ratios from this exact time period, as other proxies from the sites in which our data were collected. Please see Appendix C for an illustration of geologic time frames.

ABSTRACT

The Middle Miocene Climate Optimum was a unique warming period in the Earth's geologic history, when a high global mean annual temperature was accompanied by a relatively low global CO_2 concentration. Hydrogen isotopic signals (specifically molecular δD, the ratio of deuterium to hydrogen) from lipids of fossils and sediments offer intrinsic insights into precipitation of ancient climates. Using samples collected from known Middle Miocene deposits, we measured δD of *n*-alkanes extracted from well-preserved plant and sediment samples from varying latitudes across the Northern Hemisphere, and then analyzed the data through a zonally averaged precipitation and evaporation climate model. The reduced latitudinal temperature gradient with warm polar regions during the Middle Miocene was also contrarily coupled with a small variance in latitudinal meteoric water composition and precipitation. With our latitudinally variant sample locations (ranging from 24°N in Xianfeng, China, to 74°N in Banks Island, Canada), we developed a one-dimensional model in which we assessed evaporation and precipitation gradients throughout the Northern Hemisphere. Ultimately, we used the latitudinal distribution of δD to better constrain the atmospheric conditions during the Middle Miocene Climatic Optimum.

INTRODUCTION

In recent decades, there has been a critical push by the scientific community to better decipher the complexities of climate dynamics and variations in order to better forecasting changes within the global system. Despite the development of sophisticated three-dimensional climate models processed by supercomputers, a certain degree of uncertainty remains with regards to how certain variables (e.g. precipitation, sea levels, temperature) will respond to fluctuations in the drivers of climate change (e.g. greenhouse gas levels, solar insolation, and Milankovich cycles). By studying variations in ancient climates, or paleoclimates, we develop a better understanding of the interactions between various climate components, allowing for more accurate forecasts during the modern time period. There are several methods for reconstructing ancient climates, each relying upon direct evidence or indirect proxy data corresponding to specific dynamic characteristics, for example temperature or carbon dioxide. Our approach is to evaluate the composition of stable hydrogen isotope deuterium ("heavy hydrogen") in ancient sediment and plant fossil samples, which correlates to meteoric water content. It has been established that the deuterium composition (δD value) of evaporated water in the atmosphere is forced primarily by the initial and final temperature and pressure of the air mass at the source region and precipitation sites (Hendricks, 2000). The δD value is annotated by the following equation:

$$\delta D = 1000\,[(\mathrm{R_{SAMPLE}} - \mathrm{R_{VSMOW}})/\mathrm{R_{VSMOW}}]$$

where $\mathrm{R_{SAMPLE}}$ is the ratio of deuterium to hydrogen ($^2H/^1H$), $\mathrm{R_{VSMOW}}$ is the Vienna Standard Mean Ocean Water (VSMOW), or accepted mean $^2H/^1H$ ratio in ocean waters.

Furthermore, it is accepted that air masses, and consequently the isotopic composition at the time precipitation occurs, are governed by Rayleigh processes (Dansgaard, 1964). This theory suggests that an air parcel moves from a tropical oceanic source towards a polar region and isotopic fractionation occurs en route, with the heavy isotope content in precipitation being a unique function of both the initial isotope mass and the air parcel's water vapor mass (Jouzel, 1997).

Precipitation at any given location thus contains a signature related to the temperature and pressure in the atmosphere at the time of condensation and removal from the air parcel, having deviated from the $_{VSMOW}$ as the air mass was transported towards the poles (Dansgaard, 1964). At a given point in the pole-ward movement, precipitation is partly incorporated into the biosphere, where it is processed through the Earth's hydrologic cycle. Eventually, the rained out precipitation, containing the unique deuterium ratio, is processed by plants via root uptake, and is registered and expressed in the lipids of the leaf waxes (Yang and Leng, 2009). The δD value related to precipitation can then be discerned from the *n*-alkane in these lipids (Liu and Yang, 2006, 2008; Yang et al., 2011). However, some plant taxa may vary the isotopic composition slightly through its photosynthetic pathways or root uptake or due to different plant life forms, thus slightly altering the perceived δD precipitation value (Liu and Yang, 2008). In the absence of taxonomic information, particularly in the sediment samples, we must assume that the alteration is constant through all of our samples. Additionally, because of the exceptional preservation capabilities of lipids in leaf waxes, we are able to use the imbedded δD values as a tool for paleoclimatic evaluation (Yang and Huang, 2003).

Characteristics of the Middle Miocene Climatic Optimum

We chose to focus on the Miocene epoch, as the unique atmospheric dynamics from the Middle Miocene Climatic Optimum (MMCO) pose the potential to help understand future climatic processes. The simulated warm temperatures during the MMCO (18.4°C, approximately 3°C globally above present simulations) existed despite a relatively low CO_2 concentration (Yao, 2009) and occurred between 17 and 15 Ma (Böhme, 2003). Leading up to this event, polar regions were considerably warmer than present (Zachos et al., 2005); a mid-latitude warming of about 6°C relative to the present occurred (Flower and Kennett, 1994), resulting in a reduced equator-to-pole temperature gradient at the time of the optimum.

We set out to find what effect this reduced temperature gradient had on moisture transport to the upper latitudes and spatial distribution of deuterium through the atmosphere; without a strong polar cell blocking moisture and forcing rainout at lower latitudes, the pole-ward traveling air parcel could deliver more precipitation to high latitudes, supporting Northern Hemisphere Arctic forests that existed during and before the optimum (Witkowski, et al., 2012).

To track the rate of isotopic rainout from the air parcel moving from low to high latitudes, we employed molecular isotope analysis using gas-chromatography mass-spectrometry (GCMS) and isotope-ratio mass-spectrometry (IRMS), measuring δD of plant lipids from Northern Hemisphere sediments. The sediments, which extracted from previously dated Middle Miocene deposits, effectively average all the lipids from leaf wax from plants in the area. This is crucial to reduce any error which could be the result of different plants altering the isotopic ratio through various processes (Huang et al., 2002). Samples collected from specific plant fossil samples (e.g. *Metasequoia*), were evaluated for variations as a result of photosynthesis, root uptake, etc.

Working under the assumption described by Dansgaard (1964) that atmospheric moisture is driven by eddies and atmospheric cells from the equator/mid-latitudes to high latitudes, we correlated variations in δD values to proportional changes in latitude. That is, heavier isotopes will rainout more rapidly from the air parcel than lighter isotopes, and samples from higher latitudes should exhibit lower concentrations of deuterium, with the δD ratio becoming increasingly negative and the air parcel depleting itself of heavier isotopes (Dansgaard, 1964). However, because atmospheric deuterium content is also influenced by evaporation (i.e. evaporation replenishes the air parcel, see Figure 3) (Jouzel, 1997; Hendricks, 2000), we also evaluated the relative evaporation-precipitation (E-P) relationships latitudinally to understand where precipitation occurred during the MMCO. Evaluating the E-P ratio is critical to reconstructing atmospheric moisture, temperature, and relative humidity during the MMCO, and provides direct insight towards the characteristics of the warm upper latitude climates.

METHODS

Sample Selection and Location

Our samples were collected from previously dated Middle Miocene deposits across the Northern Hemisphere (Figure 1). In order to best capture a latitudinal trend and evaluate the equator-to-pole temperature gradient, sample sites were selected at varying latitudes, ranging from 24° N to 74° N. Considering the small sample size (n=8), we targeted locations that were more or less longitudinally unique to help achieve a mean distribution. No sample was collected from 98°W to 24°E.

These samples either consisted of sediment lipids or *in situ* lipids from exceptionally preserved *Metasequoia* and *Taxodium* leaves, as is the case with the Clarkia, Idaho, USA site. The sediment lipids, containing an accumulation of localized *n*-alkanes from various leaf waxes, were more beneficial for our purposes, as they reduced deuterium ratio variations caused by different plants. Several sample values used in this model were previously collected and measured using similar procedures and protocols (e.g. Clarkia samples, Yang and Huang, 2003).

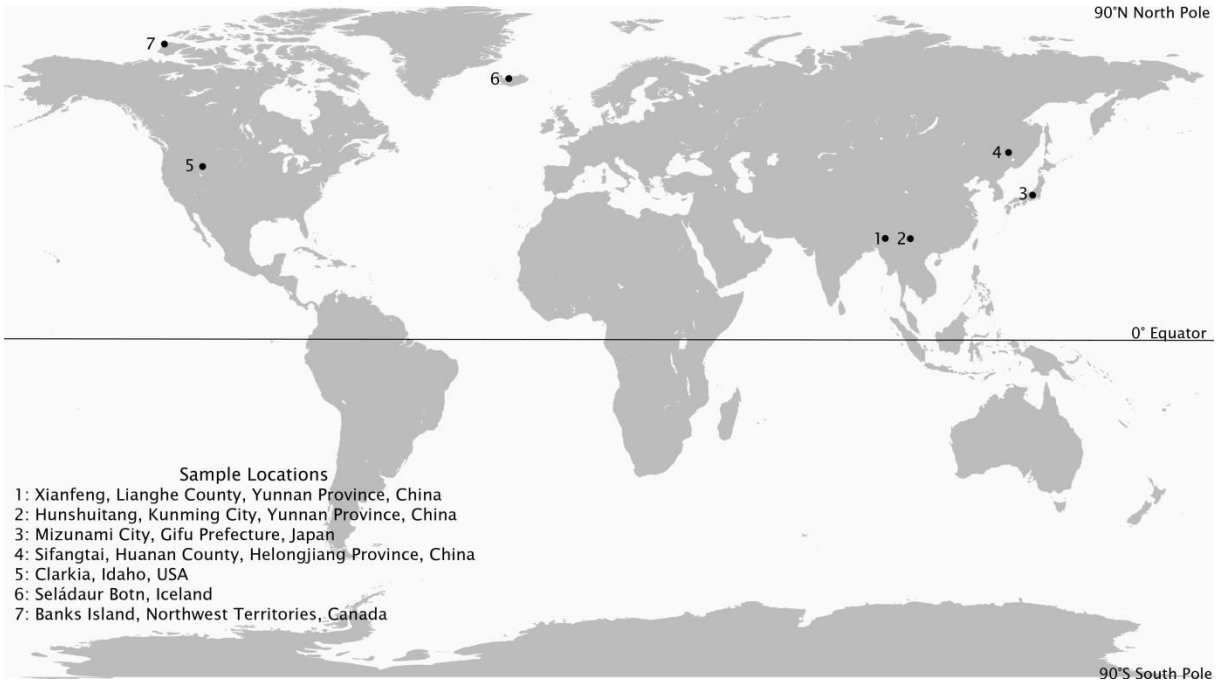

Figure 1: Sample locations from across the Northern Hemisphere.

Sample Preparation and Measurements

Lipid compounds were extracted from these samples and were evaluated for their *n*-alkane content, specifically the distribution of straight-chained carbon molecules. For the fossil samples, leaf tissue was removed and scraped from the sediment, and organic matter was crushed using a mortar and pestle. Both the sediment samples and crushed leaf samples were freeze-dried and run through the Accelerated Solvent Extractor (ASE) using a 2:1 (v/v) dichloromethane (DCM):methanol solvent mixture, effectively isolating the lipid compounds from the sample (See Appendix B for full protocols and procedures and Yang and Huang, 2003).

Following the total lipid extraction, all samples underwent silica gel flash column chromatography in which the first fraction, containing just the *n*-alkane molecules, was filtered by solvents of increasing polarity. Samples were then run through a Flame Ionization Detector (FID) on the GC to evaluate the quality and purity. Chromatographs with non-distinct peaks were urea adducted, effectively stripping cyclic and branched alkanes from the targeted straight *n*-alkanes. Samples were again processed by the FID. Evaluating the peak height produced on the chromatograph, we determined the final concentration of sample for hydrogen isotope measurement using Isotope-Ratio Mass-Spectrometer (IRMS) at Yale University (Yang et al., 2011). The final value measured by the IRMS provided us with the ratio of deuterium to hydrogen (δ 2H/1H) on three ($C\text{-}_{27}$, $C\text{-}_{29}$, and $C\text{-}_{31}$) *n*-alkane molecules (Table 1), expressed as per mil (‰). These data, coupled with latitude, allow us to construct a model simulating the meridional trend of deuterium.

Map #	Location	Coordinates	δD			Altitude (m)	Altitude Effect (+δD)	Distance to Coast (km)	Continental Effect (+δD)	Net C-29 δD
			C-27	C-29	C-31					
1	Xianfeng, Lianghe County, Yunnan Province, China	24°48'26.85"N; 98°18'3.48"E	-200.174	-221.068	-220.031	1080	20.8	720	21.6	**-178.6**
2	Hunshuitang, Kunming City, Yunnan Province, China	25° 7'57.25"N; 102°39'24.04"E	-195.708	-213.431	-213.632	2080	42.8	630	18.9	**-151.7**
3	Mizunami City, Gifu Prefecture, Japan	35°21'40.84"N;137°15'16.03"E	-181.66	-179.232	-170.068	165	1.6	48	1.4	**-176.6**
4	Sifangtai, Huanan County, Heilongjiang Province, China	46°35'0"N; 131°19'0"E	-184.666	-204.429	-198.661	159	1.0	356	10.7	**-192.7**
5*	Clarkia, Idaho, USA	46°59'31.98"N; 116°16'41.94"W	-215.954	-208	-204.212	840	15.8	782	17.9	**-174.0**
5*	Clarkia, Idaho, USA	46°59'31.98"N; 116°16'41.94"W	-210	-213	-196	840	15.8	782	17.9	**-179.3**
6	Selárdalur Botn, Iceland	65°46'16.24"N; 24° 1'39.07"W	-195.513	-191.007	-170.02	298	4.0	4	0.12	**-186.8**
7	Banks Island, Northwest Territories, Canada	74°18'N, 123°02'W	-234.127	-237	-240.685	39	0	16	0.48	**-236.7**

*Table 1: Sample sites, deuterium values, and adjusted values. *Samples were calculated by Yang and Huang, 2003.*

DATA ANALYSIS

The IRMS measurement produced a ratio of heavy hydrogen (deuterium) to hydrogen in the range of -150 to -250‰. Although this standalone value did not explicitly provide much insight, comparing relative magnitudes to other samples from the time period allowed us to establish a trend with respect to latitude. Evaluations of this trend lead to construction of our model; measuring a change in a single value, deuterium, across a linear (meridional) axis, while zonally averaging the vertical component (i.e. altitude), we developed one-dimensional analysis. This simulation provided us with an evaporation-precipitation relationship across a range of latitudes.

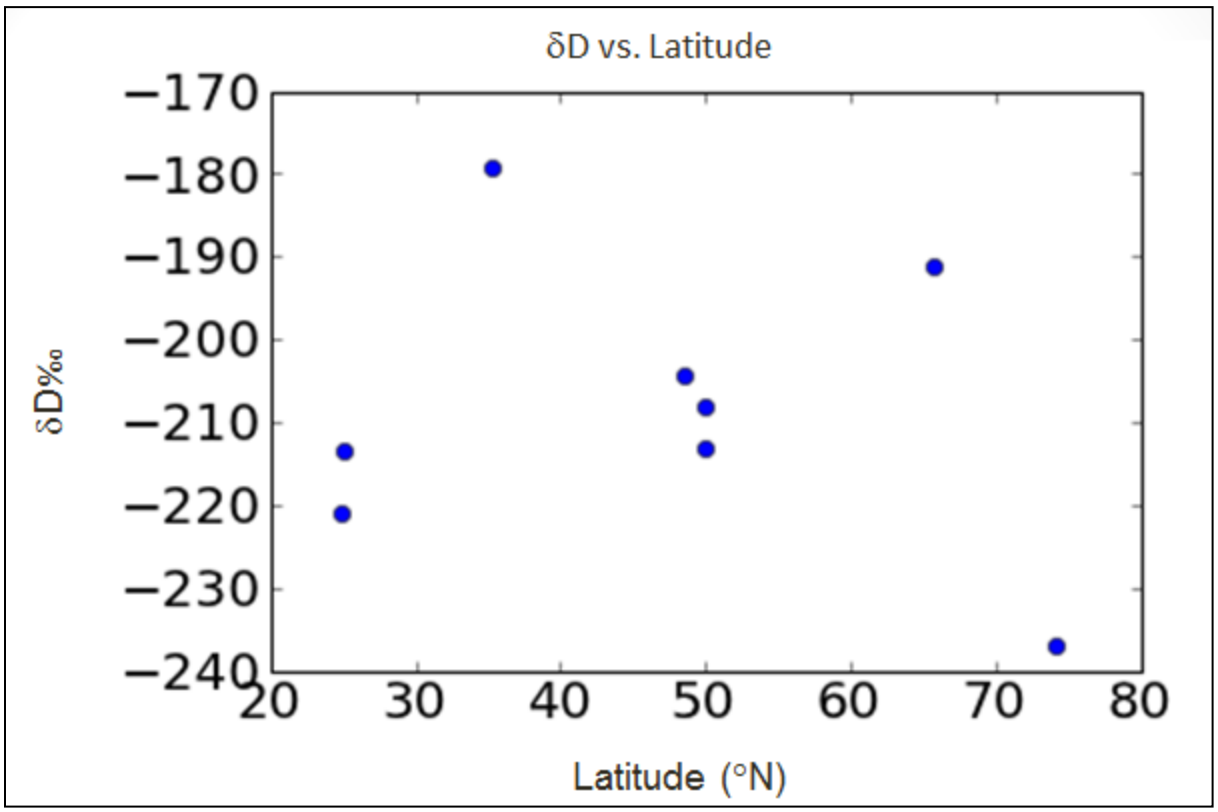

Figure 2: Plotted measured deuterium values with respect to latitude

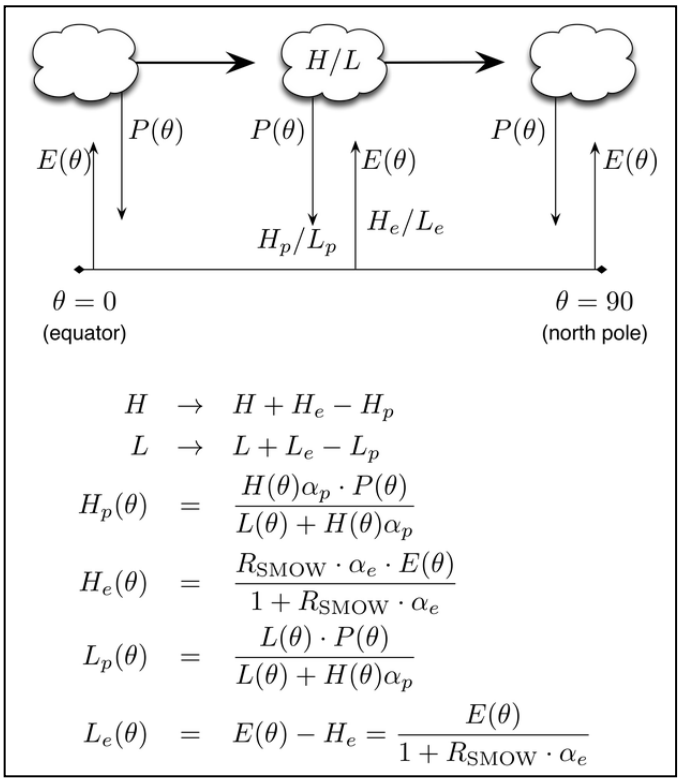

$$
\begin{aligned}
H &\rightarrow H + H_e - H_p \\
L &\rightarrow L + L_e - L_p \\
H_p(\theta) &= \frac{H(\theta)\alpha_p \cdot P(\theta)}{L(\theta) + H(\theta)\alpha_p} \\
H_e(\theta) &= \frac{R_{\mathrm{SMOW}} \cdot \alpha_e \cdot E(\theta)}{1 + R_{\mathrm{SMOW}} \cdot \alpha_e} \\
L_p(\theta) &= \frac{L(\theta) \cdot P(\theta)}{L(\theta) + H(\theta)\alpha_p} \\
L_e(\theta) &= E(\theta) - H_e = \frac{E(\theta)}{1 + R_{\mathrm{SMOW}} \cdot \alpha_e}
\end{aligned}
$$

Figure 3: Air parcel transport from the Equator to the North Pole, and equations for subsequent heavy (H) and light (L) isotope fractionation.

Figure 3 shows an illustration of Rayleigh distillation and a derivation of equations used to evaluate isotope content with respect to latitude. E(θ) and P(θ) represent the net evaporative flux or net precipitation flux at a given latitude, designated θ, ranging from 0° at the Equator to 90° at the North Pole. H is the heavy isotope concentration, and L is the light isotope concentration, where H_p/L_p and H_e/L_e are the concentrations in precipitation and evaporation respectively. $\alpha_{p/e}$ represent fractionation factors of precipitation and evaporation, and are the ratios of heavy to light isotopes of the molecule as it undergoes the process of evaporation and precipitation. The two are inverse functions of one another, such that $\alpha_e = 1/\alpha_p$. The image demonstrates an air parcel moving from the Equator to the North Pole, exhibiting the process by which isotopes are both depleted from and recharged to the air mass at any given latitude. Derivations of the equations in Figure 3 provide us with a way of simulating heavy and light isotope contents in precipitation or evaporation at any given latitude (also see Appendix D).

Model Description

Our model, written in the Python programming language, is a one-dimensional evaluation of evaporation and precipitation across a meridional axis related to δD in precipitation. We constructed two model simulations (each running for Miocene and Modern). The first interprets evaporation minus precipitation (E-P) meridionally based on the data provided by our IRMS measurements. The second model adjusted values to accommodate for additional fractionation factors in both evaporation and precipitation. These factors, proposed by Dansgaard (1964) and Jouzel (1997), allowed us to adjust the values of each specific sample to negate any geographic variations and normalize towards fractionation driven entirely by atmospheric temperature and latitude. The process is described in the "Adjusted Model Description" section.

Figure 4 expresses the Middle Miocene trend plotting deuterium values and latitude, with the modern data included for comparison. Figure 5 is a simple model simulation of the E-P relationship as latitude increases. It is important to note in both the modern simulation and Miocene simulation, E-P ratio levels off at approximately 20°N, fitting into the relatively horizontal trend provided by the data points.

The challenge of simulating the precipitation and evaporation curves by this method is that we have many unknown variables and only a handful of parameters. Therefore, we had to use modern precipitation and evaporation to roughly "sketch out" the shape of the curves, and then adjust those approximations to fit our Middle Miocene samples. It was also helpful to use temperature approximations from the MMCO (You and Huber, 2003), to aid in the illustration of temperature distributions across latitudes.

δD measurements provided us with a scattered trend that didn't exhibit any significant trend relative to latitude for Middle Miocene (see Figure 2). The δD values did consistently register more negative relative to current samples, collected from *Metasequoia* leaves (Yang et al., 2011) (Figure 4). When the two data sets are curve fitted, the negative sloping trend of the Modern samples is more plausible; the Miocene curve is more problematic, with more data points varying from the mean trend.

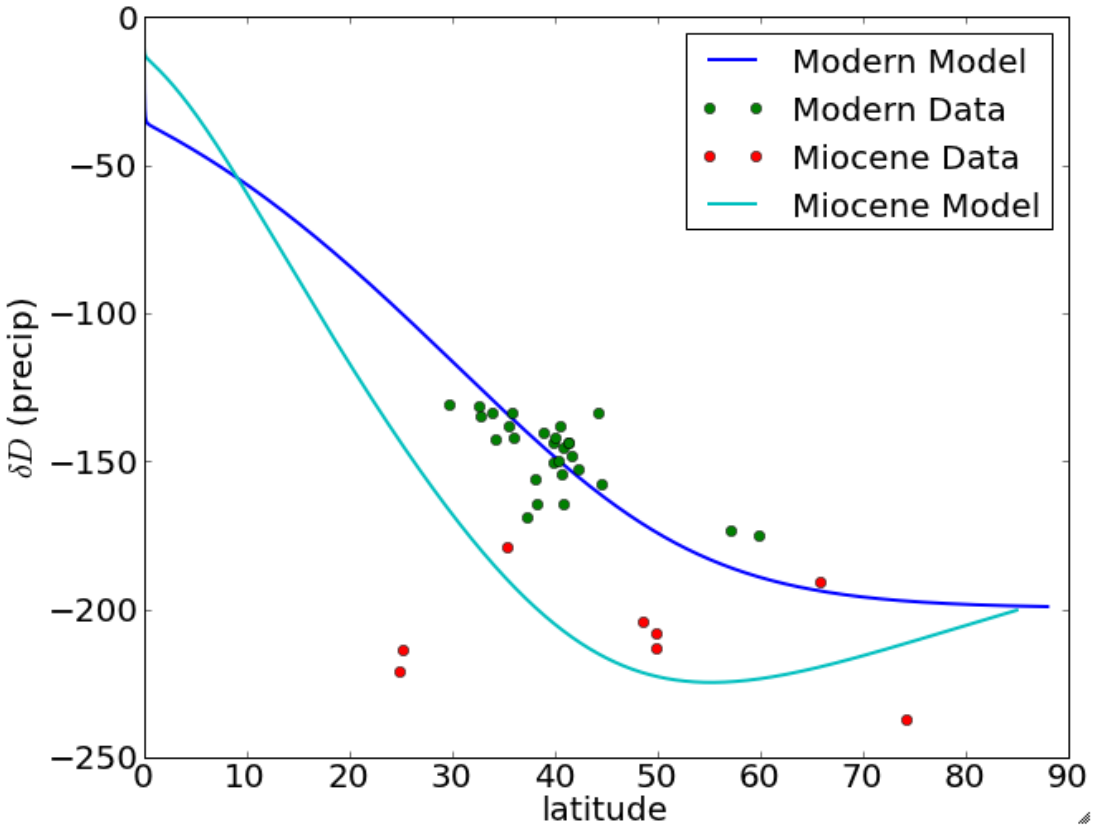

Figure 4: Plotted Modern and Miocene deuterium values with respect to latitude, and their respective models extrapolating values meridionally.

For our one-dimensional model, the vertical component can be neglected, as isotopic composition does not change with altitude (Eriksson, 1965; Hendricks, 2000). Due to the lack of data points, to best constrain the model we also eliminate the longitudinal variable; we assume longitudinal uniformity, which become more reliable after data points are adjusted.

However, this model has a peculiar increase in δD for high latitudes, likely due to the high variability in the data, resulting in a lack of any clear trend with respect to latitude. The Rayleigh model (Dansgaard 1964) of fractionation demonstrates that several characteristics of the precipitation site significantly influence the isotopic content of an air. Jouzel (1997, 2003) furthers this claim, citing a handful of factors that, in addition to latitude and air temperature, influence δD in precipitation at a given location. These factors include altitude effect, continental effect (distance to oceanic source), amount effect (quantity of precipitation), and seasonality. We

therefore adjusted our δD values accordingly based on these factors using the methods proposed by Jouzel (2003). This corrects for transport across the continental surface, and better reflects the fractionation by temperature and latitude.

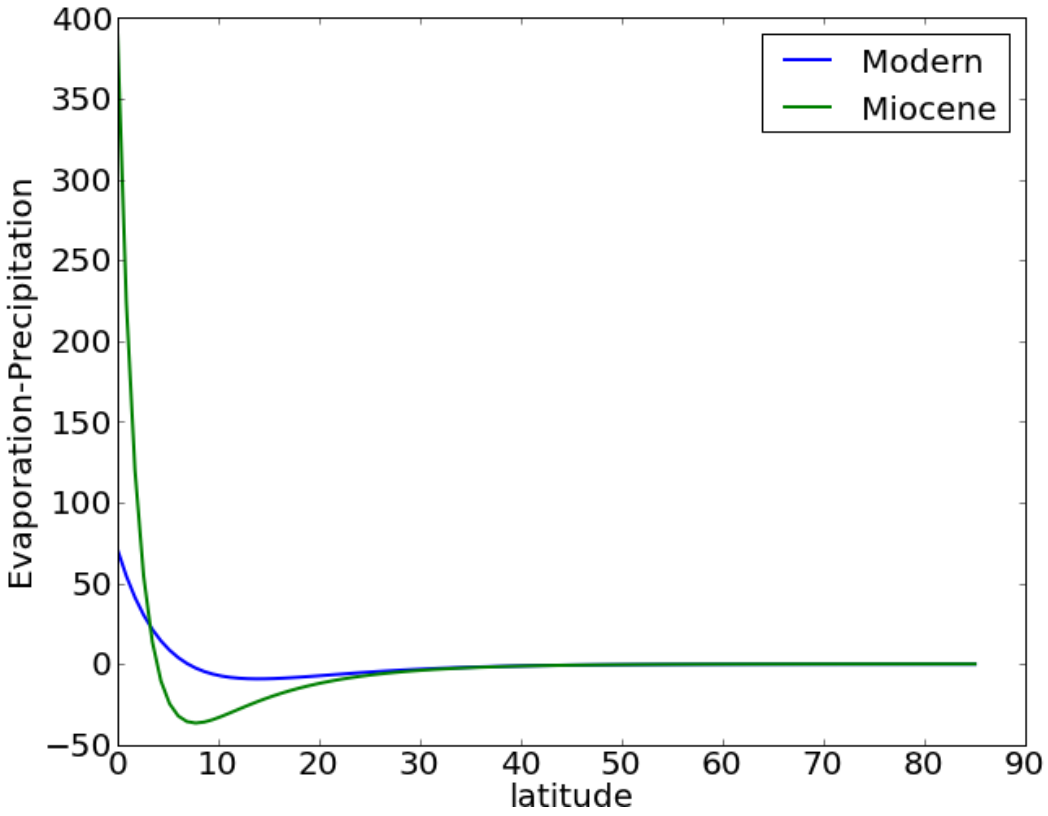

Figure 5: The relative Evaporation-Precipitation magnitudes with respect to latitude for the Modern and Miocene

Adjusting Data Points

According to Dansgaard (1964) and Jouzel et al. (1997, 2003), six variables influence the δD of a sample at a given location. They are: latitude, temperature, continental effect, amount effect, altitude effect, and seasonality. As we were attempting to evaluate hydrogen isotope fractionation based solely on two of these variables, latitude and temperature, thus we sought to nullify the other factors. In other words, as we wanted our isotope fractionation to reflect only latitude and temperature, we had to cancel out all remaining factors so as to not skew that data based on geographic discrepancies between sample locations. To do this, we used a literature

survey to find the degree to which these variables influence the δD values, and then adjusted our collected data points accordingly.

Altitude effect

Poage and Chamberlain (2001) estimated the relationship of elevation to isotope fractionation. Within a reasonable confidence interval, they are able to empirically link $\delta^{18}O$ to elevation using a linear regression. Similarly, using the Global Meteoric Water Line formula theorized by Craig (1961), we can estimate the fluctuation of deuterium in precipitation based on altitude.

Two data points that would be significantly impacted by altitude are the Xianfeng and Hunshuitang (#1 and #2 in Figure 1) which have modern elevations of 1080 meters and 2080 meters respectively. Currie (2005) and Rowley (2001) suggested that the Tibetan plateau reached its current elevation by the end of the Middle Miocene after a significant uplift in the early Miocene. Additionally, Chung et al. (1998) indicate that the southeaster edge of the Tibetan Plateau and Yangtze Block (where these samples are located) was elevated by geologic processes from the late Paleogene (40-30 Ma). It is ultimately fair to assume the altitude of these locations is roughly similar to modern day. Smiley (1985) found that the Northern Idaho region has stayed at a similar altitude since the Neogene, which includes the Miocene period. For all other data points, modern elevation is also assumed (the magnitude of δD is not that large as they have relatively low altitudes).

Using the modern elevation of these samples in the regression in Poage and Chamberlain (2001), we calculated the change in $\delta^{18}O$ with respect to altitude.

$$y = -6 \cdot 10^{-9}x^2 - 0.0027x + 0.3$$

where y is the change in $\delta^{18}O$ and x is the altitude in meters. The resulting value is a negative number that quantifies the underrepresentation caused by altitude. Since this estimates $\delta^{18}O$ and we are interested in δD, we convert our C_{-29} δD values to $\delta^{18}O$, using the linear Global Meteoric Water Line (Craig, 1961).

$$\delta D = 8.0 \cdot \delta^{18}\mathrm{O} + 10‰$$

After converting to $\delta^{18}O$, we subtracted the Poage and Chamberlain (2001) altitude adjusted values (making the value less negative), and then converted back to δD.

The Poage and Chamberlain (2001) formula is a parabolic estimation, and "zeros" or crosses the *x*-axis at 111m above sea level, such that any sample site with an elevation below this altitude would not be subject to altitude effect. Consequently, the Banks Island site (elevation of 40m) was not adjusted for altitude effect.

Continental effect

Continental effect is one of the more complex factors to estimate, as it is largely dependent upon the mechanisms for delivering precipitation to a given location, as well as seasonal patterns and orography. However, some work has been done to generally approximate δD value fluctuations based on distance from the oceanic source. Rozanski (1981) found a gradient of -3.3‰/100km in summer months and -1.3‰/100km in the winter months. Sonntag (1976, 1978) found a winter season gradient of -2.4‰/100km and a similar summer season trend, while Salati et al. (1979) found a -0.6‰/100km trend in the Amazon Basin. Considering these findings, we used a conservative approximation favoring the Rozanski summer estimation, setting the gradient to -3.0‰/100km.

The Middle Miocene saw high variance in sea levels, which were eventually stabilized following the MMCO. The highest amplitude variations occurred from ~16-14 Ma, with a movement towards a more permanent sea level fall at 14.2 Ma. This semi-permanence was likely result of the East Antarctic Ice Sheet (EAIS) growth which brought increased stability to the oceans (Flower et al. 1994). Using averages and trends from previous models, the maximum sea level may be estimated at 100m higher than present, although for modeling purposes, a conservative level is 50m in a time frame of ~15Ma (You 2009).

Thusly, for purposes of our model we assumed that sea level had little impact on continental effect, and therefore used modern day values for distance from coast. We also knew, from the locations of our data points, that sea level rise could not have been too dramatic during the MMCO as several locations are located within close proximity to the coast (as little as 4 km in the case of the Selárdalur Botn, Iceland sample). The samples that would be susceptible to substantial continental effect would be the data points [1, 2, 3, 4, 5, and 7].

We then assigned the change in δD values from continental effect, assuming current distance to the coast. The Xiangfeng City (#1 in Figure 1) is approximately 700km from the South China Sea, yielding a change of -21.6‰, Hunshuitang is 630km from its oceanic source, and thus is overrepresented by 18.9‰, Mizunami (#3) is altered by 1.44‰, Sifangtai (#4) by 10.68‰, Clarkia (#5) by 18‰, Selárdalur Botn (#6) has almost no quantifiable change (0.12‰), and Banks Island (#7) 0.48‰.

Amount effect

Amount effect is exceedingly difficult to estimate without observational data, and can only be assumed to be high in the tropics, leading to further uncertainty within this region. Therefore, we ignored amount effect while tuning our data points, instead relying upon the E(θ) and P(θ) parameters based upon modern data to model amount effect. Our lack of data at the tropics, where amount effect has the most influence on isotope fractionation, makes neglecting this variable less of a concern.

Seasonality effect

The seasonality effect may also be neglected for our purposes. Because the majority of our samples were sediment samples, seasonality is more or less neutralized. This is because our δD values were obtained from a compilation of plant leaf waxes from all plants of the area and deposited over a time transcending seasons. While it is true that these samples (particularly at the highest latitudes) may disproportionately favor spring and summer seasons (that is, when the plant is growing and absorbing groundwater), we had no clear way of defining the seasonal impact and must therefore assume that each of our samples were proportionally effected by seasonality.

After readjusting our data points to accommodate continental and altitude effect, we found that our data points follow a latitudinal gradient more closely, becoming more depleted of the heavy isotopes at high latitudes. Table 1 and Figure 6 show the newly adjusted values for the C_{-29} δD.

Modern Data

The above methods were also applied to our modern *Metasequoia* data from Yang et al., (2011) in order to run the adjusted Modern model in conjunction with the adjusted Miocene model.

Adjusted Model Description

With the adjusted data points for both modern and Miocene samples, we modeled evaporation and precipitation. We began by again plotting the deuterium values against latitude and fitting a line to reflect the data points and extrapolate to all latitudes. Figure 6 shows the Modern and Miocene plot, and it can be immediately noted that the adjusted Miocene data points better reflect high latitude distribution than the original values.

In addition to the best-fit curve, we explored the uncertainty of the parameters. Two such parameters are τ_E and τ_P the decay constant for evaporation and precipitation, respectively. In the model, these parameters determine the magnitude of evaporation and precipitation at any given latitude. The detailed forms of the evaporation and precipitation models are shown in Appendix D. In the model, some discretion was given to mirror atmospheric phenomena, mainly adding a constant to the equation of the τ_E and τ_P curves so that they do not reflect a zero value (assuming that evaporation and precipitation will always be present at a given location over an extended period of time). Additionally, a positive linear function is added to the precipitation curve to reflect increased rainout as the air parcel rains out more precipitation at higher latitudes.

Seeing that the δD value at a given location is ultimately a reflection of the evaporation and precipitation relationship, this is the only data that we could directly derive. In the absence of direct evaporation evidence, we had to look at patterns between the evaporation and precipitation and evaluate those to attempt to make a claim about a temperature trend.

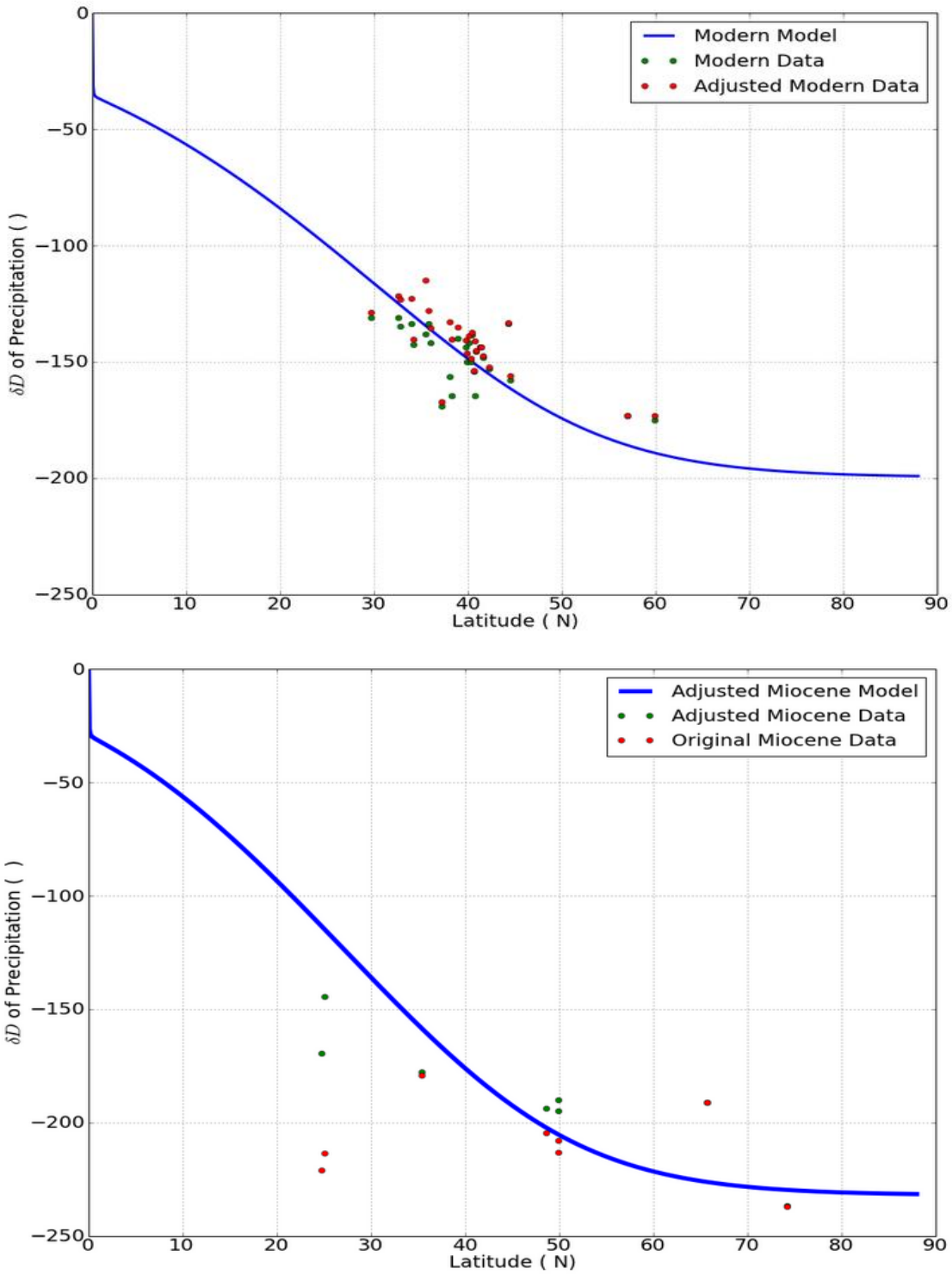

Figure 6: The original and adjusted data points and lines of best fit for the adjusted data. In the top graph showing the Modern, data points are altered only slightly. The difference is more substantial for the bottom graph depicting Miocene δD values.

With only these variables, we compared the τ_E and τ_P parameters and established a relationship between the two. Using a Bayesian Parameter estimation, we aimed to assess the significance of τ_E and τ_P, and the correlations between the two. In other words, given the data, the model estimates how the evaporation and precipitation curves are constrained. This is accomplished with a Markov Chain Monte Carlo (MCMC), a simulation technique drawing random samples from parameter probability distributions to estimate the values of τ_E and τ_P and their uncertainty, based upon the data provided. With this, the best fits and magnitude of uncertainty for τ_E and τ_P are established (see Figures 7 and 8).

The τ_E and τ_P distributions provided by the MCMC could then be run concurrently, with τ_E on one axis and τ_P on another. Run with many iterations (in this case, 20,000), a plot emerges based on the probability drawings of each parameter. Parameters that have closer relationships (e.g. both values increasing) indicate higher levels of certainty and prove correlation. A sporadic plot would imply parameter estimates that have high uncertainty and are not correlated. For τ_E and τ_P, the relationship must be well correlated, as evaporation and precipitation are generally inversely related.

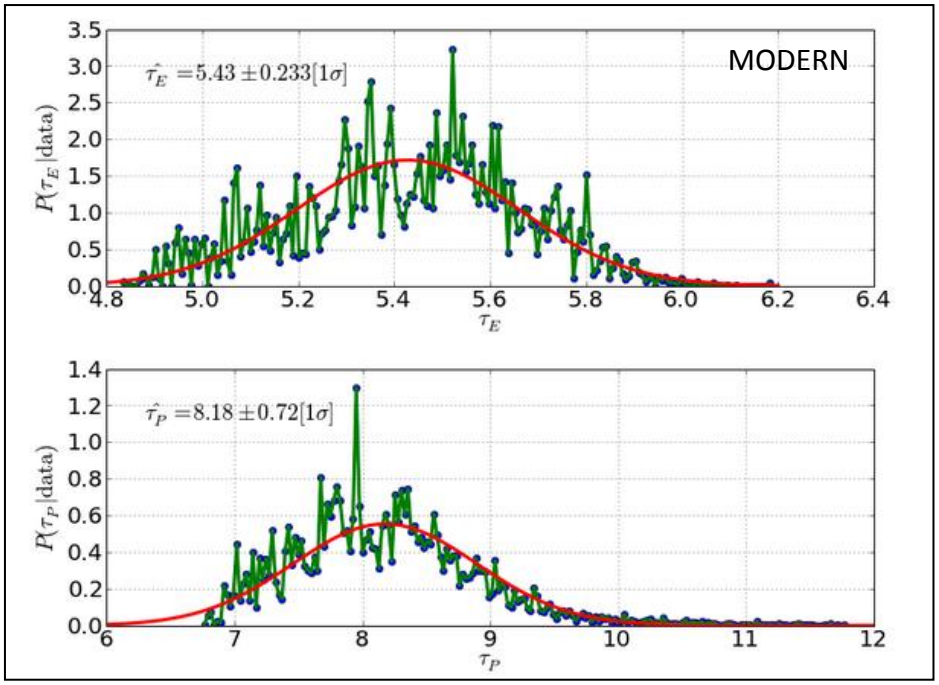

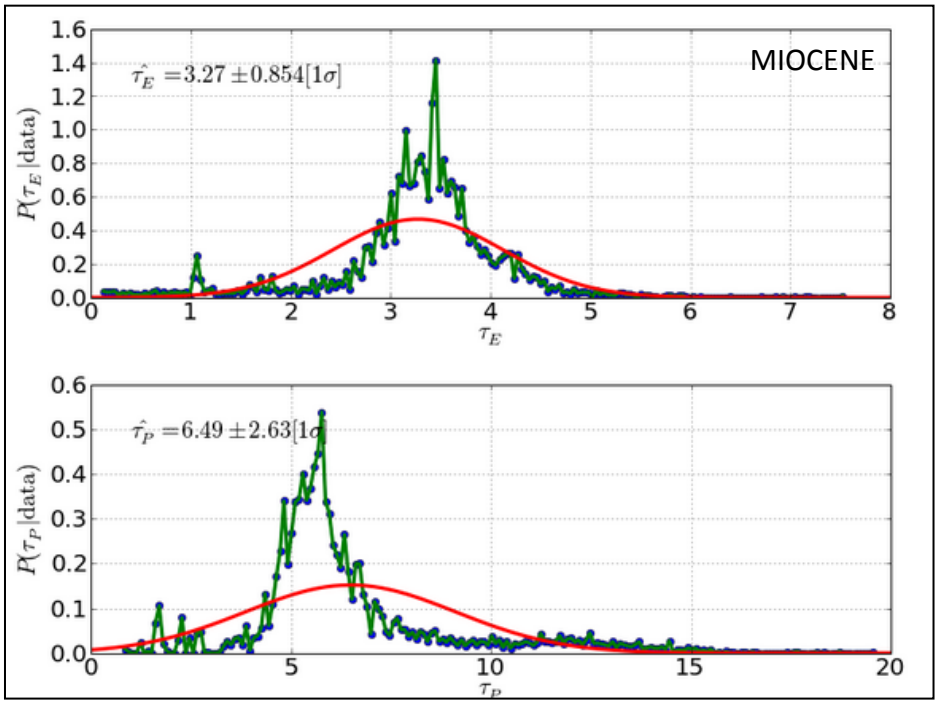

Figure 7: The probability distributions for τ_E and τ_P for the Modern and Miocene. The curves produce a range for τ_E and τ_P values, based on the data provided.

Figure 8 shows the MCMC evaluation of the Modern and Miocene simulations. It is clearly evident from comparing the two that there is a more distinct trend during the Modern, which is derived mainly from the presence of more data points, and consequently a higher confidence margin. It is important to note, however, that the Miocene MCMC still derives a fairly distinct trend in which the parameters are correlated. Despite more noise (a result of few data points), we found an equation for the relationship between τ_E and τ_P which can be used to derive both moisture and temperature distributions.

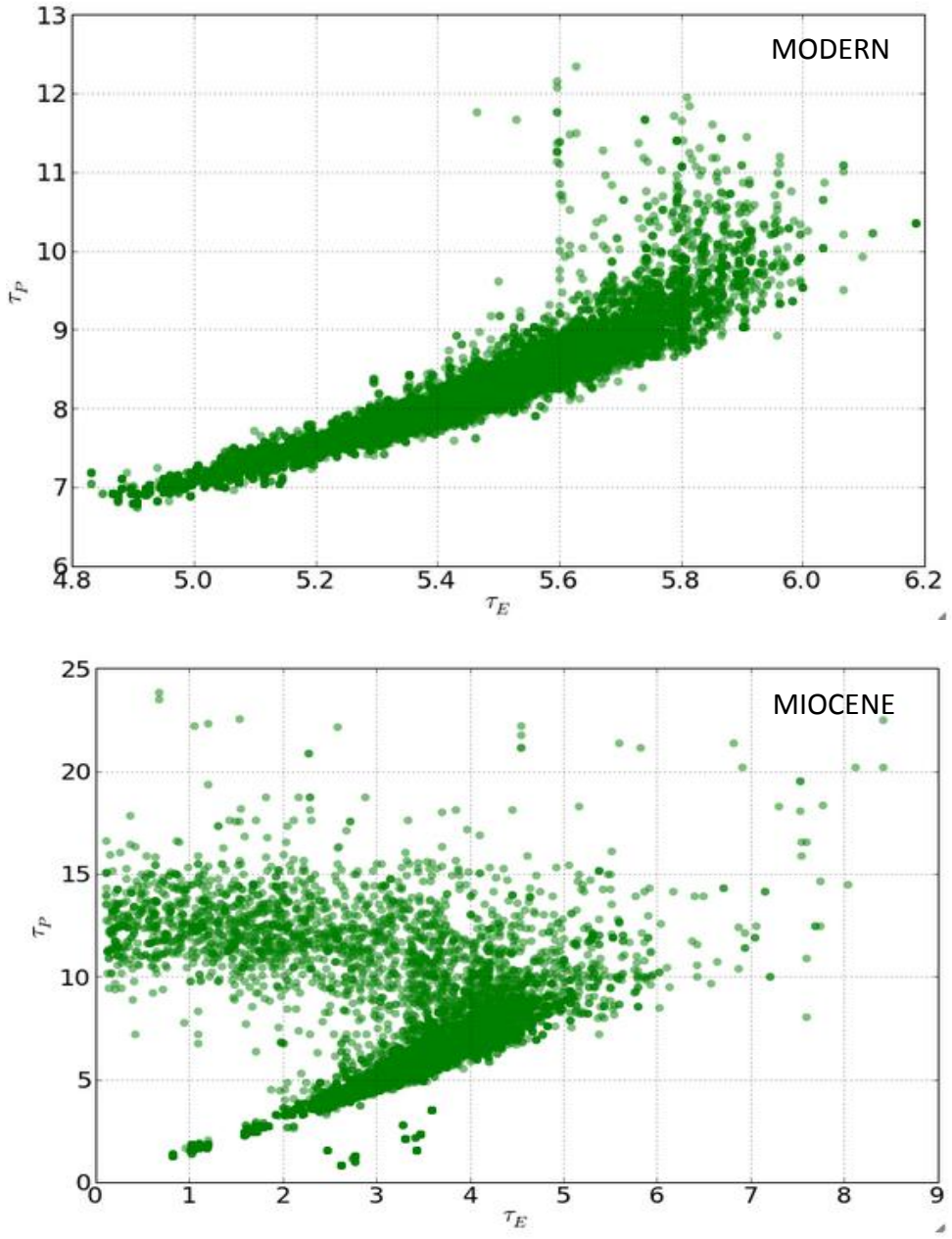

Figure 8: Plots show randomly generated τ_E and τ_P points, based on the probability distributions in Figure 7. The model was run 20,000 to develop a general trend with the assigned probabilities.

DISCUSSION

An inherent issue with paleoclimatology studies is the sensitivity of the data, which is prone to be easily misrepresented or over/underestimated. Our samples date into the millions of years, and are subject to variations from diagenetic processes, such as breakdown of organic molecules, and

geological maturity. With this in consideration, we took what we could work with, and assumed that samples undergo relatively similar lifecycles.

An example of sensitivity to myriad forcings is our Clarkia samples. Although collected from the same deposit in the same geologic time period, there exists a 5‰ δD variation. This variation could be caused by any number of things, including seasonality of the specific leaves in the fossil/sediment, plant uptake, etc. Because there is an obvious variation within latitudes, we put each of our δD values within a range of values varying from the collected data point. However, due to the lack of information, we had to assume that our collected value was the mean for the given latitude and holds equal significance to other sample values when constructing our model.

These difficulties considered, we were able to produce fairly reliable evaporation, precipitation, and temperature results. Our first model (Figure 5) indicates a stable E-P relationship across middle and high latitudes. This is to be expected in some regards, as our data points do not seem to trend with much variation in respect to latitude. Additionally, the suspected reduced temperature gradient during the MMCO would validate the E-P ratio remaining constant across latitudes, even in arctic regions where the climate likely fostered increased precipitation compared to present.

The most disconcerting aspect of the first model is in the tropics, where we see the highest E-P difference. This indicates that significant evaporation occurred within immediate proximity to the equator, and subsequent rainout ensued within 10° N latitude. This in itself is logical, as seen by the modern comparison, but the degree to which the E-P occurred it more complex. The highly positive E-P value within 5° supplies the air parcel that travels pole-ward distributing the measured isotopes. What is problematic is the lack of data collected within the tropics to confirm this model simulation. Additionally, we would expect to see E-P to become more negative at the highest latitudes where the air parcel would be primarily supplied by moisture from lower latitudes.

Evaporation and precipitation relationships are classically difficult to evaluate at low latitudes. The Intertropical Convergence Zone (ITCZ) influences seasonal rainout fluctuations and induces strong horizontal advection patterns which are difficult to capture in our 1-D model. High rates of evaporation year-round and subsequent high rates of precipitation do not allow for a strong meridional trend to develop within the range of 0° to 10° N. The latitudinal temperature gradient is small in these latitudes, and relatedly so is water content relative to latitude (Hendricks, 2000). The stability of this region, regardless of climatic variations in mid and high latitudes, makes linking gradient variations <10° difficult to extent to higher latitudes. Furthermore, a lack of Middle Miocene proxy data further complicates simulation. Therefore, we must use our data from the middle and high latitudes to project the positive E-P flux within the tropical zone. Although this method does not necessarily yield accurate representation for these latitudes, it does satisfy the development of our model, as we can approximate the flux and use it as a parameter for net rainout in middle latitudes.

Some difficulty also arises in producing explicit, stand-alone results. We worked only with two parameters, evaporation and precipitation, and therefore had no way of assessing the exact magnitude of these values. That is, we could not produce a value dictating the specific amount of evaporation we have a given location. We could, however, sum up the relative E and P curves with respect to one another and to the Modern simulation. Without the assistance of other parameters to refine our evaporation and precipitation, all subsequent results were relative.

When we ultimately ran the adjusted model, we began to develop a better picture of evaporation and precipitation with respect to latitude, as well as improve our confidence intervals for parameter correlation. Our simple plot (Figure 6) showed a much more promising and intuitive δD curve across latitudes than our first rendering (Figure 4). Seeing a trend that more closely mimicked Modern data indicated a step in the right direction. The running of the MCMC chain showed a high correlation between the τ_E and τ_P parameters (for both Modern and Miocene). Even despite the small data set of eight, we were able to find well correlated parameters and a reliable model.

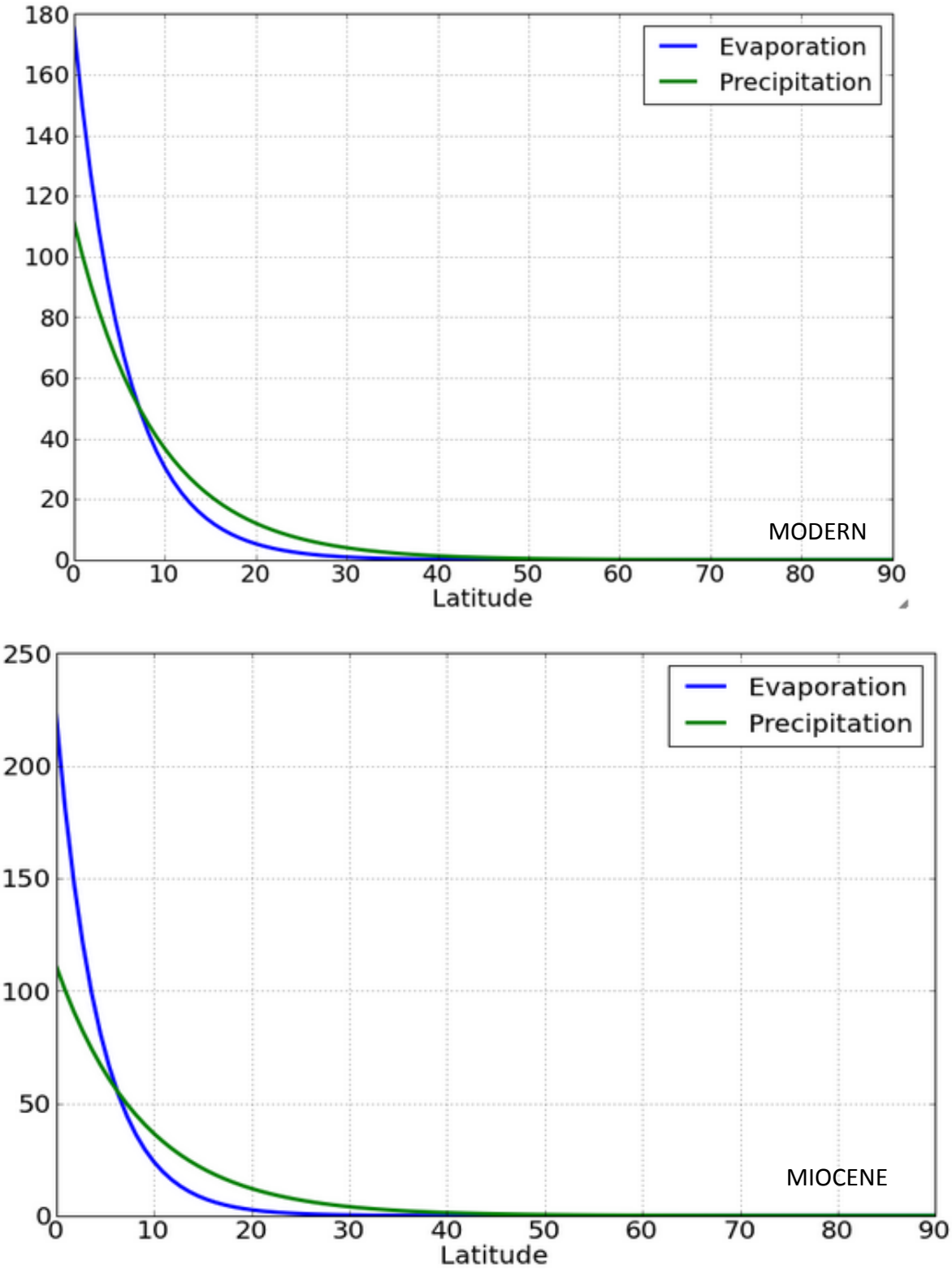

Figure 9: The adjusted Modern and Miocene Evaporation and Precipitation curves based on the τ values from Figures 7 and 8.

Figures 9 and 10 highlight the final derivations of evaporation and precipitation for both the Modern and the Miocene. Comparing Modern data to the Miocene, we saw low latitude evaporation is significantly greater during the Miocene. The low τ_E value indicates that a substantial portion of MMCO evaporation took place at the Equator, more so than it does today. This means, in terms of a relative temperature distribution, the Equator region (within 10°-15°) saw a heightened temperature increase. Furthermore, from Figures 7-9, the relatively higher Miocene τ_P matches the hypothesis that the magnitude of precipitation was greater at mid- and high-latitude locations.

Additionally, Figure 10 shows the "steep" Miocene evaporation curve, indicative of the warm equatorial zones, before plateauing quickly. The quantity of evaporation is lower and the gradient reduced through latitudes north of 15°, more so than the Modern. This matches the proposed reduced temperature gradient of the MMCO. By evaluating the Figure 10 precipitation curves, we see precipitation is of greater magnitude than the Modern at low latitudes (to match the high evaporation), but also better projects precipitation into the high latitudes, beginning around 25°N. This trend, coupled with the higher τ_P value, points to a reduced Miocene precipitation gradient compared to the Modern. This matches the reduced temperature gradient, and relates to more precipitation reaching the polar regions.

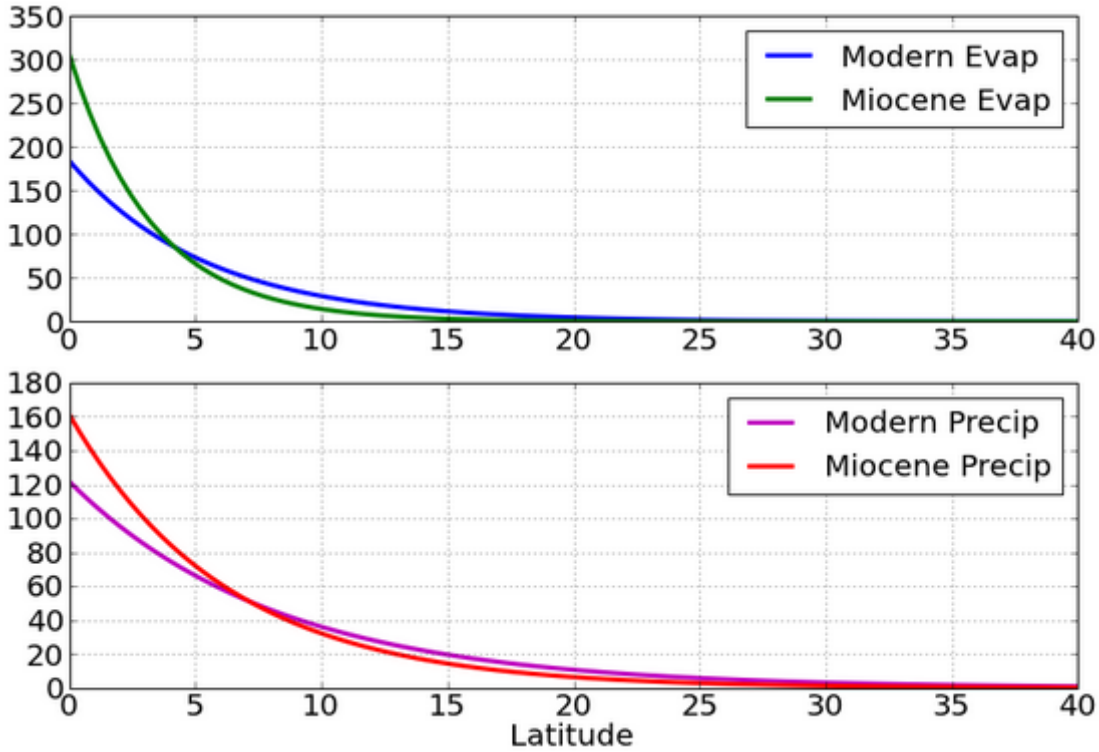

Figure 10: A comparison of the Modern and Miocene evaporation and precipitation curves, and their respective magnitude relative to latitude.

CONCLUSIONS

Finding the τ_E and τ_P for both the Modern and the Miocene, we found the relative distributions of evaporation and precipitation across a latitudinal axis. The Modern τ_E approximation is larger than the Miocene estimation, indicating that evaporation has a relatively higher magnitude at lower latitudes during the Miocene. This implies that, compared to mid- to high-latitudes, more evaporation occurs at the equator than during the Modern. We also saw a lower τ_P during the Miocene than during the Modern. This correlates to higher precipitation at higher latitudes, a rainout pattern that could only exist with a small temperature gradient. That is, a sharper temperature gradient at the upper latitudes, similar to today, would prevent much precipitation from reaching the polar regions. With our significant and correlated τ_E and τ_P, we found that the temperature distribution during the Miocene concentrated most of the heat at lower latitudes, and then evenly distributed that trend up to the poles. Although we were unable to find explicit

temperature values, we were able to develop a fairly detailed picture of relative evaporation, precipitation, and temperature distributions and gradients during the MMCO.

ACKNOWLEDGEMENTS

We would like to thank the NASA Rhode Island Space Grant for funding of this project, the Bryant University Department of Science and Technology for use of their facilities and equipment. I am grateful for Dr. Gerard Olack and Mr. Glendon Hunsinger of Yale University's Earth System Center for stable Isotopic Studies for technical support on hydrogen isotope measurements, Dr. Xiaoyan Ruan of China University of Geoscience at Wuhan and a visiting scholar at Bryant University for processing samples, Dr. Zekun Zhou (Kunming Botanical Institute and Xishuangbanna Botanical Garden, Chinese Academy of Sciences), Dr. Chris Williams (Franklin and Marshall College), and Dr. Fridgeir Grimsson (University Vienna)for providing samples. Dr. Dan McNally served as a reviewer and read an early version of the manuscript.

REFERENCES

Böhme, M., 2003. The Miocene Climatic Optimum: evidence from ectothermic vertebrates of Central Europe. Palaeogeography, Palaeoclimatology, Paleoecology, 195: 389-401.

Bowen, G.J. and Revenaugh, J., 2003. Interpolating the isotopic composition of modern meteoric precipitation. Water Resources Research, 39(10, 1299): SWC 9-1~13.

Chung, S.L., Lo, C.H., Lee, T.Y., Zhang, Y., Xie, Y., Li, X., Wang, K.L., Wang, P.L., 1998. Diachronous uplift of the Tibetan plateau starting 40 Myr ago. Nature, 394: 769-773.

Craig, H., 1961. Isotopic variations in meteoric waters. Science, 133(3465): 1702-1703.

Currie, B.S., Rowley, D.B., Tabor, N.J., 2005. Middle Miocene paleoaltimetry of southern Tibet: Implications for the role of mantle thickening and delamination in the Himalayan orogen. Geology, 33(3): 181-184.

Dansgaard, W., 1964. Stable isotopes in precipitation. Tellus, 16(4): 436-468.

Eglinton, T., G. Eglinton, 2008. Molecular proxies for paleoclimatology. Earth and Planetary Science Letters, 275: 1-16.

Eriksson, E., 1965. Deuterium and ^{18}O in precipitation and other natural waters; some theoretical considerations. Tellus, 27: 498-512.

Farquhar, G.D., Cernusak, L.A., 2007. Heavy water fractionation during transpiration. Plant Physiology, 143: 11-18.

Flower, B.P. and Kennett, J.P., 1994. The middle Miocene climatic transition: East Antarctic ice sheet development, deep ocean circulation and global carbon cycling. Palaeogeography, Palaeoclimatology, Paleoecology, 108: 537-555.

Gat, J.R., 1996. Oxygen and hydrogen isotopes in the hydrologic cycle Annu. Rev. Earth Planet. Sci., 24: 225-262.

Henderson-Sellers, A., K. McGuffie, and Wiley, 1987. A Climate Modeling Primer.

Hendricks, M.B., D.J. DePaolo, R.C. Cohen, 2000. Space and time variation of $\delta^{18}O$ and δD in precipitation: Can paleotemperature be estimated from ice cores? Global Biogeochemical Cycles, 14(3): 851-861.

Holbourn, A., Kuhnt, W., Schulz, M. and Erlenkeuser, H., 2005. Impacts of orbital forcing and atmospheric carbon dioxide on Miocene ice-sheet expansion. Nature, 438: 483-487.

Huang, Y., Shuman, B., Wang, Y., Webb T III, 2002. Hydrogen isotope ratios of palmitic acid in lacustrine sediments record late-quaternary climate variations. Geology, 30: 1103-1106.

Jakobsson, M. et al., 2007. The early Miocene onset of a ventilated circulation regime in the Arctic Ocean. Nature, 447: 986-990.

Joussame, S., Sadourny, R. and Jouzel, J., 1984. A general circulation model of water isotope cycle in the atmosphere. Nature, 311: 24-29.

Jouzel, J., Alley, R.B., Cuffey, K.M., Dansgaard, W., Grootes, P., Hoffmann, G., Johnsen, S.J., Koster, R.D., Peel, D., Shuman, C.A., Stievenard, M., Stuiver, M., White, J., 1997. Validity of the temperature reconstruction from water isotopes in ice cores. Journal of Geophysical Research, 102(C12): 26,471-26,487.

Jouzel, J., Vimeux, F., Caillon, N., Delaygue, G., Hoffman, G., Masson-Delmotte, V., Parrenin, F., 2003. Magnitutde of isotope/temperature scaling for interpretation of central Antarctic ice cores. Journal of Geophysical Research: Atmospheres, 108(D12).

Kavanaugh, J.L., Cuffey, K.M., 2003. space and time variation of $\delta^{18}O$ and δD in Antarctic precipitation revisited. Global Biogeochemical Cycles, 17(1): 1-14.

Kürschner, W.M., Kvaček, Z. and Dilcher, D.L., 2008. The impact of Miocene atmospheric carbon dioxide fluctuations on climate and the evolution of terrestrial ecosystems. Proceedings of the National Academy of Sciences, USA (PNAS), 105(2): 449-453.

Lee, J.E., Fung, I., DePaolo, D.J., Henning, C.C, 2007. Analysis of the global distribution of water isotopes using the NCAR atmospheric general circulation model. Journal of Geophysical Research: Atmospheres, 112(D16).

Leng, Q. and Yang, H., 2010. A new approach to reconstruct Paleogene atmospheric hydrology at high latitudes. Science Foundation in China, 17(2): 46-49.

Leng, Q., Yang, H., Wang, L. and Li, C.-X., 2009. Discovery and evolution history of *Metasequoia*. In: J.-G.e.-i.-c. Sha (Editor), Centennial Celebration of Chinese Palaeontology. Science Press, Beijing, pp. 360-368 (in Chinese).

Liu, W.-G. and Yang, H., 2008. Multiple controls for the variability of hydrogen isotopic compositions in higher plant n-alkanes from modern ecosystems. Global Change Biology, 14: 2166-2177.

Liu, W.-G., Yang, H. and Li, L.-W., 2006. Hydrogen isotopic compositions of n-alkanes from terrestrial plants correlate with their ecological life forms. Oecologia, 150: 330-338.

Merlivat, L., Jouzel, J., 1979. Global Climatic Interpretation of the Deuterium-Oxygen 18 Relationship for Precipitation. Journal of Geophysical Research, 84(C8): 5029-5033.

Moberg, A., Sonechkin, D.M., Holmgren, K., Datsenko, N.M., Karlen, W., 2005. Highly variable Northern Hemisphere temperatures reconstructed from low- and high-resolution proxy data. Nature, 433(7026): 613-617

Micheels, A., Bruch, A.A., Uhl, D., Utescher, T. and Mosbrugger, V., 2007. A Late Miocene climate model simulation with ECHAM4/ML and its quantitative validation with terrestrial proxy data. Palaeogeography, Palaeoclimatology, Palaeoecology, 253: 251-270.

Müller, R.D., Sdrolias, M., Gaina, C., Steinberger, B., Heine, C., 2008. Long-Term Sea-Level Flucturations Driven by Ocean Basin Dynamics. Science, 319(5868): 1357-1362.

Nathan, S.A. and Leckie, R.M., 2009. Early history of the Western Pacific Warm Pool during the middle to late Miocene (~13.2-5.8 Ma): Role of sea-level change and implications for equatorial circulation. Palaeogeography, Palaeoclimatology, Paleoecology, 274: 140-159.

Osborne, C.P., 2008. Atmosphere, ecology and evolution: what drove the Miocene expansion of C_4 grasslands? Journal of Ecology, 96(1): 35-45.

Poage, M.A., Page Chamberlain, C., 2001. Empirical Relationships Between Elevation and the Stable Isotope Composition of Precipitation and Surface Waters: Considerations For Studies of PaleoElevation Change. American Journal of Science, 301: 1-15.

Rogl, F., 1999. Mediterranean and Paratethys. Facts and Hypotheses of an Oligocene to Miocene Paleogeography (short overview). Geologica Carpathica, 50: 339-349.

Royer, D.L. et al., 2001. Paleobotanical evidence for near present-day levels of atmospheric CO_2 during part of the Tertiary. Science, 292(5525): 2310-2313.

Rozanski, K., Sonntag, C., Munnich, K.O., 1982. Factors controlling stable isotope compostion of European precipitation. Tellus, 34: 142-150.

Shevenell, A.E., Kennett, J.P. and Lea, D.W., 2004. Middle Miocene Southern Ocean Cooling and Antarctic Cryosphere Expansion. Science, 305: 1766-1770.

Sokolov, A.P. and Stone, P.H., 1998. A flexible climate model for use in integrated assessments. Climate Dynamics, 14: 291-303.

Solomon, S. et al., 2007. Climate Change 2007: The Physical Science Basis. Contribution of Working Group I to the Fourth Assessment Report of the Intergovernmental Panel on Climate Change. Cambridge University Press, Cambridge, UK and NY, USA: .

Sonntag, C., Neureuther, P., Kalinke, C., Münnich, K., Klitzch, E., Weistroffer, K., 1976. Paläoklimatik der Sahara- Ontinentaleffekt im Dund ^{18}O-Gehalt pluvialer Saharawässer. Naturwissenschaften, 63: 497.

Sonntag, C., Klitzsch, E., Shazly, E.M., Kalinke, C., and Münnich, K.O., 1978. Paläoklimatische Information im Isotopen-gehalt ^{14}C-datierter Saharawässer: Kontinentaleffekt in D und ^{18}O. Geol. rundsch, 67: 413-423.

Speelman, E.N., Sewall, J.O., Noone, D., Huber, M., von der Heydt, A., Sinnighe Damste, J., Reichart, G. , 2010. Modeling the influence of a reduced equator-to-pole sea surface temperature gradient on the distribution of water isotopes in the Early/Middle Eocene. Earth and Planetary Science Letters, 298: 57-65.

Sturm, C., Zhang, Q. and Noone, D., 2010. An introduction to stable water isotopes in climate models: benefits of forward proxy modeling for paleoclimatology. Clim. Past, 6: 115-129.

Verducci, M. et al., 2009. The Middle Miocene climatic transition in the Southern Ocean: Evidence of paleoclimatic and hydrographic changes at Kerguelen plateau from planktonic foraminifers and stable isotopes Palaeogeography, Palaeoclimatology, Paleoecology, 280: 371-386.

Wang, C., Zhao, X., Liu, Z., Lippert, P.C., Graham, S.A., Coe, R.S., Yi, H., Zhu, L., Liu, S., Li, Y., 2008. Constraints on the early uplift history of the Tibetan Plateau. PNAS, 105(13): 4987-4992.

White, J.W., 2004. Paleoclimate. Do I hear a million? Science, 304(5677): 1609-1610.

Witkowski, C., Gupta, N.S., Yang, H., Leng, Q., Williams, C.J., Briggs, D.E.G., and Summons, R.E., 2012. Molecular preservation of Cenozoic conifer fossil lagerstatten from Banks Island, the Canadian arctic. Palaios, 27: 279-287.

Yang, H., Blais, B. and Leng, Q., 2011. Stable isotope variations from cultivated *Metasequoia* trees in the United States: A statistical approach to assess isotope signatures as climate signals. Japanese Journal of Historical Botany (Special Issue of the proceedings of the Third International *Metasequoia* Symposium, August 3-8, 2010, Osaka, Japan), 19(1-2): 75-88.

Yang, H. and Huang, Y.-S., 2003. Preservation of lipid hydrogen isotope ratios in Miocene lacustrine sediments and plant fossils at Clarkia, northern Idaho, USA. Organic Geochemistry, 34: 413-423.

Yang, H. and Leng, Q., 2009. Molecular hydrogen isotope analysis of living and fossil plants - *Metasequoia* as an example. Progress in Natural Science, 19: 901-912.

Yang, H., Liu, W.-G., Leng, Q. and Hren, M.T.P., Mark, 2011. Variation in n-alkane δD values from terrestrial plants at high latitude: Implications for paleoclimate reconstruction. Organic Geochemistry, 42: 283-288.

Yao, M.S., Stone, P.H., 1987. Development of a Two-Dimensional Zonally Average Statistical-Dynamical Model. Part 1: The Parameterization of Moist Convection and its Role in the General Circulation. Journal of the Atmospheric Sciences, 44(1): 65-82.

You, Y., Huber, M., Muller, R.D., Poulsen, C.J. and Ribbe, J., 2009. Simulation of the Middle Miocene Climate Optimum. Geophysical Research Letters, 36: 1-5.

Zachos, J., Pagani, M., Sloan., Thomas, E., Billups, K., 2001. Trends, Rhythms, and Aberrations in Global Climate 65 Ma to Present. Science, 292: 686-693.

AFTERWORD

In our eyes, this multi-stage, interdisciplinary project successfully took a limited number of Middle Miocene data points and created a working model simulating evaporation and precipitation. Starting with fossil and sediment samples that served as proxies for climate during the 15-17 million years, we were able to construct a latitudinal distribution of δD values related to precipitation. Although deposits containing MMCO climatic information is sparse, we ultimately produced eight samples that sufficiently served our purposes.

We next purified the fossils and sediments and isolated the exact compounds related to hydrogen isotope fractionation. At the end of the laboratory phase of the project, we had explicit δD values related to given latitudes. From these δD values, we were able to derive the relationship between evaporation and precipitation ranging from the Equator to the North Pole, and ultimately tie that back into the temperature distribution of the time period.

The modeling phase was met with some setbacks, but in the end these issues were resolved by adjusting our Miocene data points so that the δD values only reflected latitude and air temperature. With this tuning made, we saw an intuitive δD with respect to latitude, and were able to proceed with our model.

Through a process of parameter estimation, we arrived at our final results for distribution of evaporation and precipitation, and relatedly, temperature. Most simply, our results showed that during the Middle Miocene Climatic Optimum, the Earth was substantially warmer than Modern; although, most of that heat was centered in the equatorial regions. Evaporation and precipitation were also very high in these areas. However, as latitude increases and moves towards the poles, evaporation drops off sharply, and precipitation is well distributed into the poles. In other words, from the middle latitudes up to the North Pole, the precipitation and temperature distributions are fairly balanced, more so than today.

This information presents value to the scientific community as a way of understanding the processes related to atmospheric moisture transport and the relationships of evaporation and temperature in a climate different than today. During the Middle Miocene, with a climate warmer

than Modern, the variations in magnitude and distribution of evaporation, precipitation, and temperature may be an example of a future climate that we may soon be facing. It is important to understand the relationship of these variables to garner better insight towards how the climate behaves under certain conditions; consequently, we are satisfied with our contribution to this discussion, and believe that the results we concluded can contribute to a greater cause of understanding the Earth's climate.

APPENDICES

Appendix A: Glossary

Term	**Explanation**
δD	Read "delta D," this correlates to an empirical data point representing the difference ratio of deuterium to hydrogen in a sample. It follows the equation: $\delta D = 1000[(R_{SAMPLE} - R_{VSMOW})/ R_{VSMOW}]$
Advection	A process by which meteoric water is moved through the atmosphere. Advection is the bulk transport of a substance through a medium. In this case, advection is the process by which an air parcel is moved through the atmosphere, transporting with it hydrogen isotopes.
Air mass	See "Air parcel"
Air parcel	A theoretical mass of atmospheric moisture that is transported by advective and diffusive forces (i.e. by temperature and pressure differences). In this context, it is assumed that an air parcel moves from the equator towards the poles, driven primarily by advective processes. It is also from the air parcel that precipitation containing a unique isotope signature is rained out.
Altitude effect	A factor of isotope fractionation in precipitation in which locations at higher altitude will be more depleted of heavy isotopes.
Amount effect	A factor of isotope fractionation in precipitation in which locations with high amounts of precipitation will have relatively higher abundances of heavy isotopes.
Atmosphere	One of the four interconnected "spheres" of the Earth. Relating to the gases (including water vapor) within the gravitational range of the Earth.
Biosphere	One of the four interconnected "spheres" of the Earth. Relating to all living things and ecosystems.
Carbon dioxide	A greenhouse gas emitted from the combustion of fossil fuels. It is suggested its emission is responsible for modern day global warming. See also: "Greenhouse gas."
Climate	The sum of the parts of: precipitation, temperature, humidity, wind and atmospheric pressure at a given location over an extended period of time.

Continental effect	A factor of isotope fractionation in precipitation in which locations further from the ocean will be more depleted in heavy isotopes
Deuterium	They heavy isotope of hydrogen, containing 2 isotopes. May also be referred to simply as "D" or "^{2}H" in context. Deuterium is often present in the atmosphere and biosphere in the form of heavy water, or HDO (as opposed to H_2O).
Diffusion	A process by which meteoric water is moved through the atmosphere. Diffusion is the transport of a substance through a medium without bulk motion. In this case, diffusion is the process by which hydrogen isotopes are transported through the atmosphere, although not necessarily within a bulk air mass. In other words, diffusion would evenly distribute deuterium molecules throughout the atmosphere in the absence of air parcel transport.
East Antarctic Ice Sheet	Abbreviated EAIS, it is a section of Antarctica on the ocean. The expansion and retraction of this ice sheet is has served as an indicator of global climate.
Eddies	A circulation pattern that serves as a "ball-bearing" of sorts, moving in the opposite direction of the drivers next to it. For example, a Ferrell cell, located in-between Hadley and Polar cells, circulates air in the opposite direction as its neighbors.
Epoch	A length of time on the geologic scale, shorter than a period but longer than an age.
Ferrell cell	An atmospheric circulation pattern that sits in between, and is largely dependent upon, the Hadley and Polar cells, as it exists as an eddy.
Fossil fuels	Fuels from ancient biological matter created from chemical processes over millions of years. The burning of these substances (including coal and oil) generate electricity but also emits greenhouse gases into the atmosphere.
Fractionation	The process by which a mixture is divided into fractions. Isotopic fractionation is the process by which isotopes are separated from their original solution. In the context of this research, isotopic fractionation is the separation of water molecules containing deuterium from those containing hydrogen in the atmosphere.

Geosphere	One of the four interconnected "spheres" of the Earth. Relating to the rocks, soil, and geologic portions of the Earth.
Global Circulation Model	Also referred to as a GCM, this is a computer generated model that analyzes data points from across the globe to create a 3-dimensional reconstruction of the Earth's climate. Although often criticized for their flaws, often in the form of over/under signifying variables or physical equations, GCMs are the most useful tool for simulating future climate scenarios.
Global Meteoric Water Line	The average relationship between hydrogen and oxygen isotopes in water worldwide. The generally accepted equation is: $\delta D = 8.0*\delta^{18}O + 10‰$.
Greenhouse gas (effect)	A gas that is released into the atmosphere and subsequently prevents radiated heat from escaping the Earth. Higher levels of greenhouse gases in the atmosphere relate to more heat being trapped, causing the temperature of the Earth to rise.
Hadley cell	An atmospheric circulation pattern that moves rising air from the Equator and transports it poleward at a higher elevation, until returning the air to the surface and area of high pressure, usually in the mid-latitudes.
Hydrologic cycle	How water moves through the different spheres of the Earth. Most simply, the process of evaporation from the surface, transport through the atmosphere, precipitation, transport through the geosphere, hydrosphere, and biosphere, ultimately returning to the atmosphere through evaporation on a perpetual cycle.
Hydrosphere	One of the four interconnected "spheres" of the Earth. Relating to the movement of water throughout the atmosphere, geosphere, and biosphere.
in situ	Latin for in position, this refers to a specimen or sample that has not been moved or altered from its initial position.
Isotope	An alteration in the number of neutrons in an element. For example, a hydrogen atom most commonly contains 1 proton, 1 neutron, and 1 electron. An isotope of hydrogen is deuterium, or heavy hydrogen, which has 1 proton, 2 neutrons, and 1 electron.
Isotope gradient	The amount by which the isotope ratio changes over a given frame of

	reference; in this case, the difference between isotope ratios at varying latitudes.
Isotope ratio	The ratio between a specific isotope and its most abundant form. In this case, the ratio between deuterium and hydrogen (the most abundant form).
Isotopic fractionation	See "Fractionation"
Isotopic signature	The isotope ratio at a given point, relating to its intrinsic characteristics. In this case, the ratio pertaining to evaporation and precipitation at a given location.
Latitude	A geographic coordinate, being a theoretical band on the Earth's surface that denotes relative North or South location and runs east-west, parallel to the Equator. 0° signifies the Equator, with 90°N and 90°S marking the geographic North and South Poles respectively.
Latitudinal gradient	The change in latitude between two points.
Lipid	A classification type for molecules. Naturally occurring, lipids include fats, sterols and waxes, among others. Lipids are found on the surface of leaves and intrinsically hold the isotopic signature of water from root uptake. Additionally, lipids are preserved extremely well over long time frames, making it a valuable proxy when evaluating climates millions of years old.
Longitude	A geographic coordinate, being a theoretical band on the Earth's surface denoting relative East or West location running north to south, parallel to the Prime Meridian. 0° signifies the Prime Meridian, ranging to 180° eastward and westward
Meridionally	Along a meridian; travelling across latitudes
Metasequoia	A deciduous redwood tree. An ancient tree, this species has great value for paleoclimatology, as the isotopic content of lipids preserved in its leaves correlate well to deuterium in the atmosphere.
Meteoric water content	The isotope and moisture content of water in the atmosphere at a given time and location.

Middle Miocene	A geologic timeframe occurring from 16-11.6 million years ago. It is a sub-epoch of the Miocene, both of which occurred during the Neogene. See also Appendix C.
Milankovitch cycles	Changes in the Earth's movements that influences global climate. The cycles include eccentricity (the shape of the Earth's orbit around the sun), obliquity (the tilt of the Earth relative to its orbital plane), and axial precision (rotation of Earth's axis). All three have marked cycles on the magnitude of several ten-thousand year periods, and are believed to play a large role in the cyclical ice age patterns.
n-alkane	A straight-chained molecule containing carbon and hydrogen atoms.
Orography /orographic features	Relating to mountain building processes and crustal uplift
Paleoclimate	An ancient climate.
Polar cell	An atmospheric circulation pattern that upwells air at mid-latitude (modern day is approximately 60°N/S) and moves it through the atmosphere, eventually returning it to the surface at the pole.
Protium	The most naturally occurring isotope of hydrogen. May also be referred to simply as hydrogen, or hydrogen's "light" isotope.
Proxy	A piece of data that quantitatively relates to a piece of information about an ancient climate
Rainout	Precipitation heavy isotopes from the atmosphere at a given time and location
Relative humidity	The ratio between the partial pressure of water vapor and its saturated vapor pressure. Dependent upon temperature and air pressure, relative humidity is an important factor in the rates of evaporation and precipitation.
Seasonality	A factor of isotope fractionation in precipitation in which different seasons yield varying levels of heavy isotopes. It can be expected that during winter months, precipitation will be more depleted of heavy isotopes relative to summer months.

SMOW	See "Vienna Standard Mean Ocean Water"
Solar insolation	The amount of radiation from the sun at a given location over a certain period of time. Solar insolation is prone to fluctuations from the sun's energy output, and has an effect on the Earth's climate.
Temperature gradient	The rate at which temperature changes between two points. In the context of an Equator-to-Pole temperature gradient, it is the slope between the temperature at the equator and the North/South pole.
Vienna Standard Mean Ocean Water	The accepted mean $^{2}H/^{1}H$ ratio in ocean waters. The current standard, as evaluated by the International Atomic Energy Agency is 155.76 ± 0.1 ppm.
VSMOW	See "Vienna Standard Mean Ocean Water"
Well-preserved	A sample that has not been subject to decay or weathering, making it a candidate for use as a paleoclimate proxy.

Appendix B: Chromatographs

The following graphs provide readouts printed by Yale University's IRMS relating to our δD measurements. Each peak relates to a certain carbon chain, and the number on the peaks to the relative abundance of the compounds in those chains. From this, the IRMS is able to provide a ratio between deuterium and hydrogen, giving us our δD values. The information above each graphic relates the map number in Figure 1, and the location of the sample.

#1, Xianfeng, Lianghe County, Yunnan Province, China

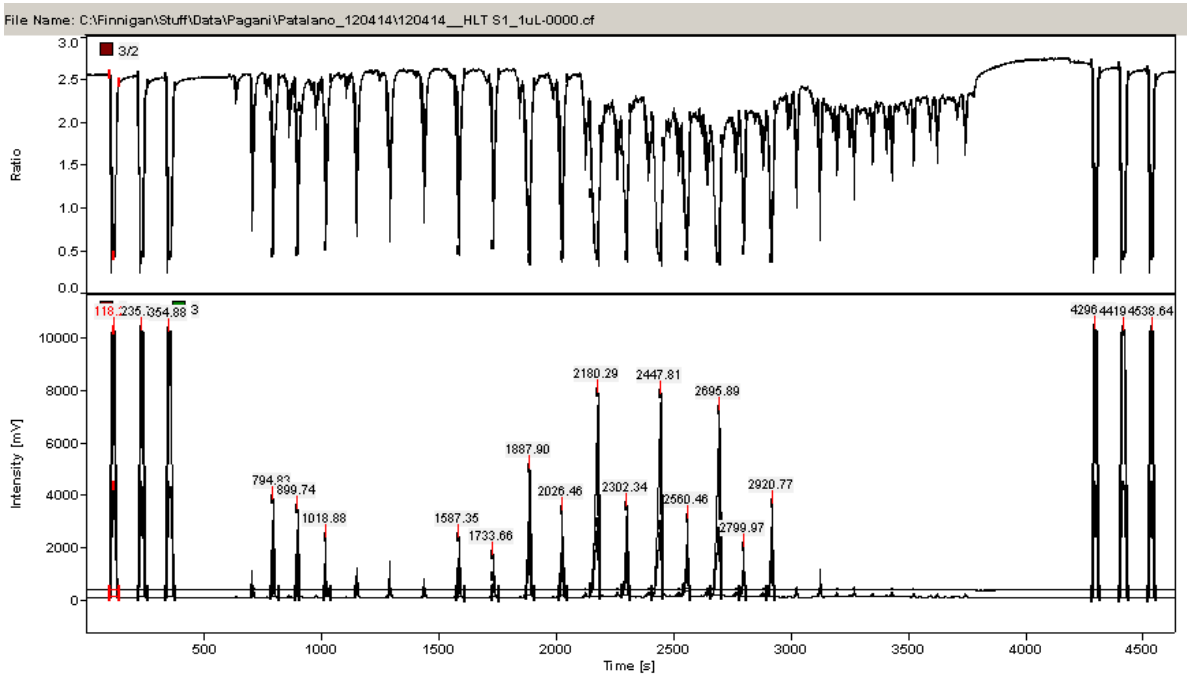

#2, Hunshuitang, Kunming City, Yunnan Province, China

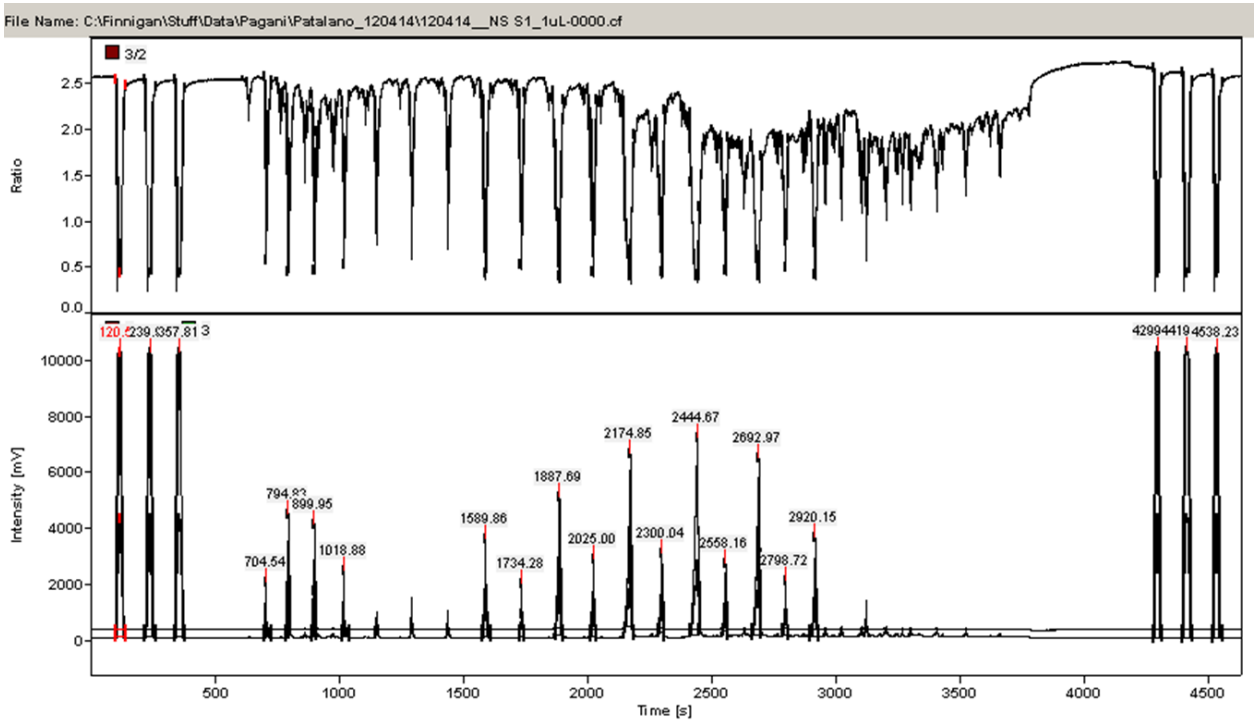

#3, Mizunami City, Gifu Prefecture, Japan

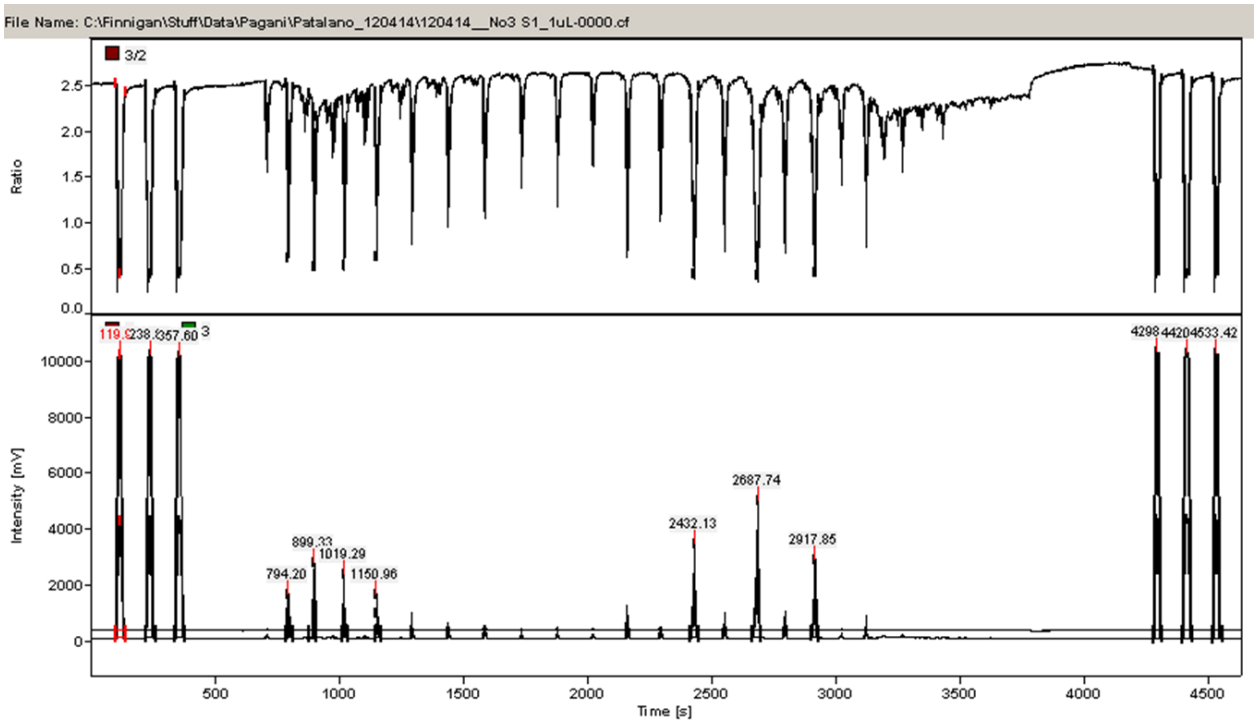

#4, Sifangtai, Huanan County, Heilongjiang Province, China

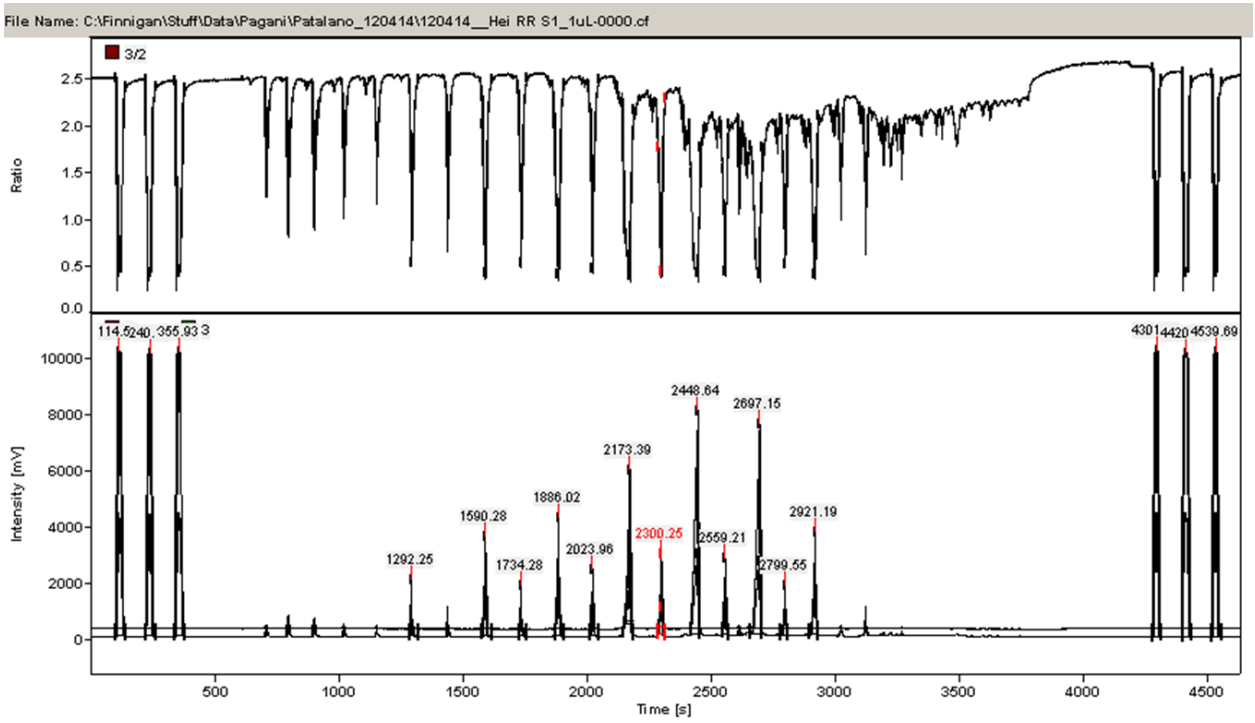

#6, Selárdalur Botn, Iceland

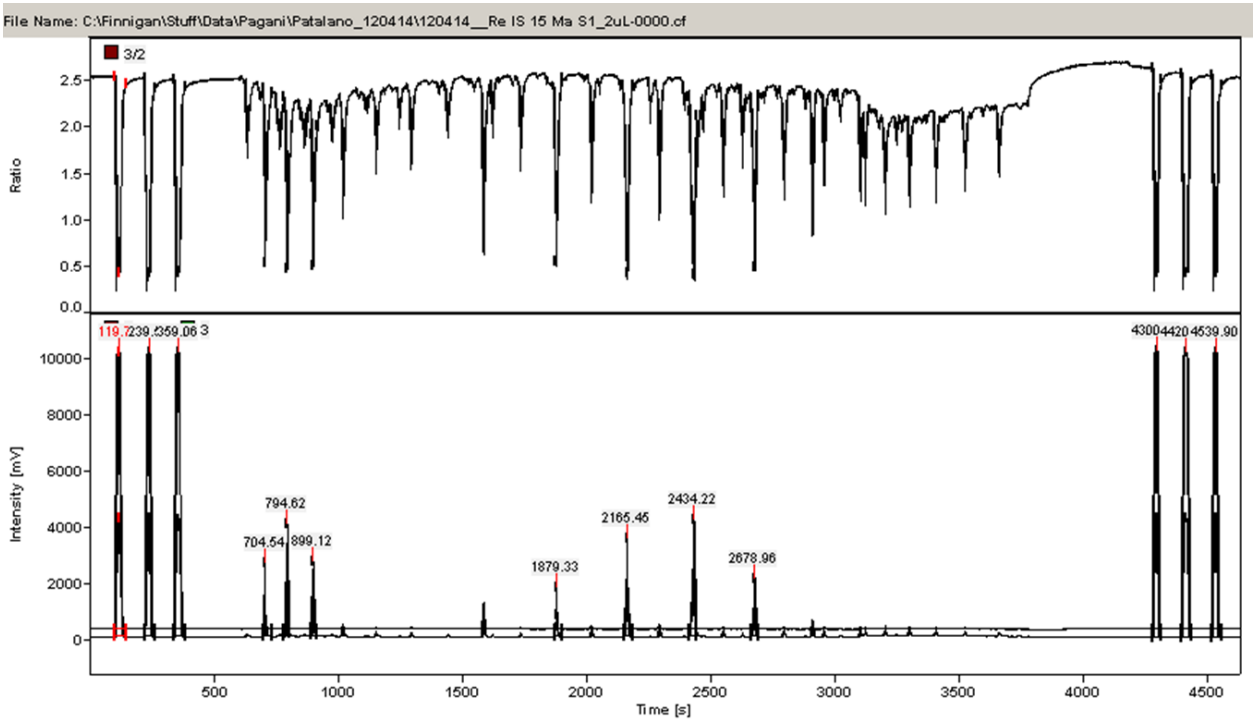

Appendix C: Geologic Time Periods

The following page shows a stratigraphic visualization of all the geologic time periods. The graph is read from the top left, down the column, and then to the top right of the next column. "Age" refers to the age from present, in millions of years (Ma).

Both the modern geologic time period and the Miocene occurred during the Cenozoic era. The Miocene epoch occurs during the first part of the Neogene Period. The Miocene epoch is informally broken down into three "sub-epochs," the Early, Middle, and Late Miocene. The Middle Miocene was comprised of two ages, first the Langhian, and then the Serravallian.

The modern geologic time period is in the Quaternary Period, and Holocene epoch, which extends back approximately 12,000 years. Although controversial, a new proposal (albeit informal) is to delineate a new epoch entitled the "Anthropocene" referring to the most recent, man-made alterations to the climate.

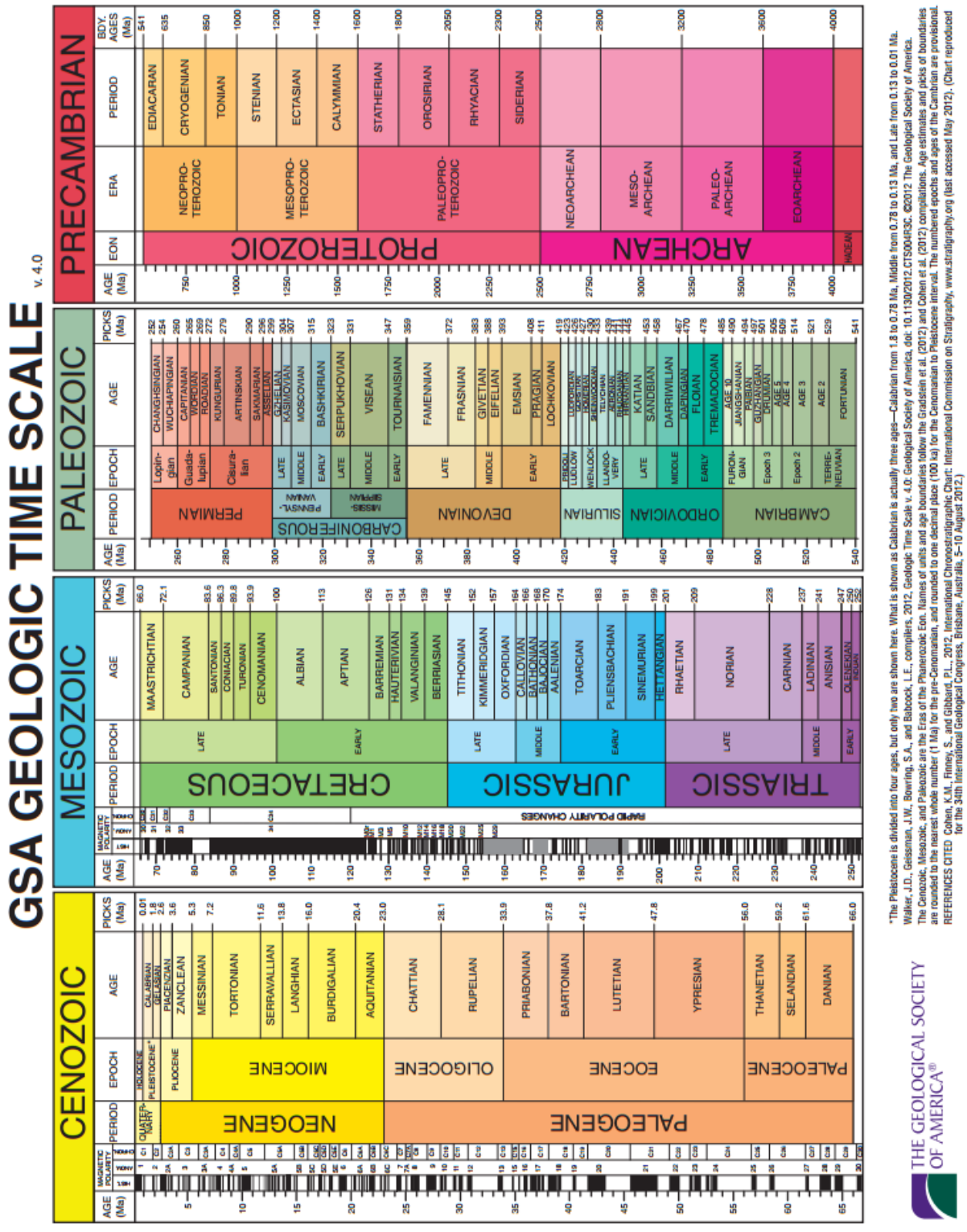

*The Pleistocene is divided into four ages, but only two are shown here. What is shown as Calabrian is actually three ages—Calabrian from 1.8 to 0.78 Ma, Middle from 0.78 to 0.13 Ma, and Late from 0.13 to 0.01 Ma.

Walker, J.D., Geissman, J.W., Bowring, S.A., and Babcock, L.E., compilers, 2012, Geologic Time Scale v. 4.0: Geological Society of America, doi: 10.1130/2012.CTS004R3C. ©2012 The Geological Society of America.

The Cenozoic, Mesozoic, and Paleozoic are the Eras of the Phanerozoic Eon. Names of units and age boundaries follow the Gradstein et al. (2012) and Cohen et al. (2012) compilations. Age estimates and picks of boundaries are rounded to the nearest whole number (1 Ma) for the pre-Cenomanian, and rounded to one decimal place (100 ka) for the Cenomanian to Pleistocene interval. The numbered epochs and ages of the Cambrian are provisional.

REFERENCES CITED Cohen, K.M., Finney, S., and Gibbard, P.L., 2012, International Chronostratigraphic Chart: International Commission on Stratigraphy, www.stratigraphy.org (last accessed May 2012). (Chart reproduced for the 34th International Geological Congress, Brisbane, Australia, 5–10 August 2012.)
Gradstein, F.M., Ogg, J.G., Schmitz, M.D., et al., 2012, The Geologic Time Scale 2012: Boston, USA, Elsevier, DOI: 10.1016/B978-0-444-59425-9.00004-4.

Appendix D: Model Details

Evaporation and precipitation equations:

$$E(q) = E_o \exp(-t / t_E) / t_E + E_1$$
$$P(q) = P_o \exp(-t / t_P) / t_P + P_1 + (P_2 - P_1) q / 90^o$$

Simulation parameters:

t_E	1-40 (fit)
t_P	1-40 (fit)
P_o	1000
P_1	0
P_2	0
E_o	1000
E_1	0

Python Code for Simulation:

```
sim=Simulation()

tau_E=4.5  # only difference with Modern

sim.add("EE=E(t,tau_E,Eo,E1)",plot=False)
sim.add("PP=P(t,tau_P,Po,P1,P2)",plot=False)
sim.add("RR=R(t,R_SMOW)")

sim.add("Lp=L*PP/(L+H*alpha_prec)")
sim.add("Hp=H*alpha_prec*PP/(L+H*alpha_prec)")

sim.add("He=RR*alpha_evap*EE/(1+RR*alpha_evap)")
sim.add("Le=EE/(1+RR*alpha_evap)")


# determine extra = integrated E-P - doesn't seem to work
sim.params( Eo=Eo,
            E1=E1,
            tau_E=tau_E,
            tau_P=tau_P,
            Po=Po,
            P1=P1,
            P2=P2
            )

H0=R_SMOW*alpha_evap*extra/(1+R_SMOW*alpha_evap)
L0=extra-H0

```

```
29. sim.add("H'=He-Hp",H0,plot=False)
30. sim.add("L'=Le-Lp",L0,plot=False)
31. 
32. sim.add("N_vapor=L+H")
33. sim.add("R_vapor=H/L")
34. sim.add("R_precip=Hp/Lp")
35. 
36. sim.add("delta=(R_vapor/R_SMOW-1)*1000",plot=False)
37. sim.add("delta_precip=(R_precip/R_SMOW-1)*1000",plot=True)
38. 
39. sim.params(alpha_evap=alpha_evap,
40.             alpha_prec=1/alpha_evap,
41.             R_SMOW=R_SMOW,
42.             )
43. 
44. dataset='Adjusted Miocene'
45. x,y=mydata[dataset]['Latitude'],mydata[dataset]['d']
46. sim.add_data(t=x,delta_precip=y,plot=True)
47. 
48. sim.functions(E,P,R)
49. sim.run(0,88)
```